Title:

Targeting CERS6-AS1/FGFR1 axis as synthetic vulnerability to constrain stromal cells supported proliferation in Mantle cell lymphoma

Introdution:

Mantle cell lymphoma (MCL) is indeed recognized as an aggressive and incurable subtype of B-cell neoplasm where nearly 60% of patients presented bone marrow involvement at the time of diagnosis and causes significant morbidity due to relapse disease (1). Various therapeutic options for MCL treatment including standard-of-care R-CHOP, targeted therapies such as Bruton's tyrosine kinase (BTK) inhibitors, and Chimeric antigen receptor T-cell therapy are available (2,3). However, the selection of treatment depends on the patient's age, disease stage, and associated comorbidities. Despite of available therapies, resistance cases emerge rapidly due to various reasons, such as loss or mutation in drug targets like loss of CD19 expression or BTK gene mutation. The presence of inherently chemo-resistant tumor-initiating cells can also be a probable cause (2,4-7). In addition, the complex network and interaction between the bone marrow microenvironment and MCL cells provide specific niches for lymphoma cells survival (8-12). Therefore, discovery of substantial clinically relevant targets and new therapies are needed to eliminate the supportive niche provided by tumor microenvironment (TME), which will possibly enhance the efficacy of existing MCL treatments (13-15).

Immune escape and acquired therapy resistance are the current two major obstacles towards successful cancer treatment those are also associated with immunosuppressive microenvironment (16, 17). Besides therapies targeting protein-coding genes, several studies have identified intracellular or extracellular RNA molecules, including long non-coding RNAs (lncRNAs), that regulates gene expression by influencing chromatin organization, alternative splicing, RNA decay, transcription, and led to tumor progression (16, 18). Although their identification in lymphoma has been limited, over the past decade, eight studies have highlighted the role of lncRNAs in MCL (19, 20). Elevated expression of MALAT1 and ROR1-AS1, has been observed in MCL compared to healthy donor B-cells those regulate gene transcription by associating with PRC2 complex (21, 22). FOXP4-AS1 contribute to MCL proliferation and invasion through the miR-423-5p/NACC1 pathway (23). Downregulated lncRNAs in MCL, such as GATA6-AS and MORT, regulate MCL cell proliferation by altering GLUT1 and miRNA-16 expression respectively and regulating MCL cells apoptosis (24, 25). While lncRNAs have demonstrated prognostic value in MCL and could serve as potential therapeutic targets, current studies have not emphasized their role in reprogramming the TME.

CERS6-AS1, transcribed from the CERS6 gene (2q24.3), has gained considerable attention in various cancer types over the past three years (26). It is consistently upregulated in multiple cancers including pancreatic, papillary thyroid, colorectal, breast, gastric, and hepatocellular carcinoma, and correlating with unfavorable clinical outcomes (27-33). Its oncogenic mechanism primarily involves sponging miRNAs, and thereby regulating downstream miRNA-targets (26). Additionally, interactions with RNA-binding proteins IGF2BP3 contribute to

CERS6-AS1 regulation (34). Beyond affecting cancer cell proliferation, invasion, and apoptosis, CERS6-AS1 influences the stemness of colorectal cancer cells (31).

We have investigated the oncogenic functions of CERS6-AS1 which is upregulated in MCL and in MCL/stromal cells co-culture model and associated with poor overall survival. Specifically, we found CERS6-AS1 promotes interaction between RNA-binding protein nucleolin and FGFR1 transcript, impacting its stability. Moreover, we discovered that genetic knockdown of CERS6-AS1 in MCL cell lines or pharmacological inhibition of nucleolin in combination with FGFR1 inhibition resulted in suppression of CERS6-AS1 associated cancer stem cell phenotype and promoted MCL cells killing in protective MCL/stromal cells co-culture model.

Objectives:

- To investigate the role of CRES6-as1 long non coding RNA in MCL: focusing on its interaction with tumor microenvironment.
- To provide mechanistic insights into regulatory network involving CERS6-AS1, nucleolin, and FGFR1 axis-associated crosstalk between tumor cells and stromal cell interaction and identifying the therapeutic potential of targeting a non-coding RNA in MCL.

Materials and Methods:

Patient samples

Peripheral blood from healthy donors and blood, lymph nodes, bone marrow, and formalin-fixed paraffin-embedded (FFPE) tissue from MCL patients were obtained from medical hospitals including All India Institute of Medical Science (AIIMS), Rishikesh; Sanjay Gandhi Post Graduate Institute of Medical Sciences (SGPGI), Lucknow; and King George's Medical University (KGMU), Lucknow, India. Clinical information, including age, gender, B-symptoms, extranodal involvement, and survival outcomes, were collected and recorded. Diagnosis of MCL was based on the expression of CD5+ and CD19+ markers in conjunction with the expression of cyclin D1 and/or detection of t(11;14) translocation by cytogenetics or fluorescence *in situ* hybridization analysis. This study followed the institutional human ethical guidelines standards of CSIR-Central Drug Research Institute (CDRI), Lucknow (CDRI/IEC/2023/PA13).

B-cells isolation

B-cells from peripheral blood from healthy donor's or leukemic phase of MCL were isolated by Histopaque-1077 (Sigma Aldrich, 10771) gradient centrifugation followed by using negative selection based untouched B-cell isolation magnetic beads (Miltenyi Biotec, 130031151). Isolated B-cells were counted, re-suspended in a freezing medium containing 90% foetal bovine serum (FBS) (Gibco, 26140079) and 10% dimethyl sulfoxide (Sigma Aldrich, D2650) and stored in liquid nitrogen until use. CD5+ naïve B-cells were isolated from whole blood from healthy donors by FACS sorting. In brief, red blood cells were removed by Histopaque-1077. The isolated peripheral blood mononuclear cells (PBMCs) were stained for four markers: CD3-,

CD45-FITC, CD19-PE and CD5-BV421. Sorted CD3-CD45+CD19+CD5+ cells underwent RNA extraction for further molecular analysis.

Cell culture, primary MCL/MS5 stromal cell co-culture and drugs MCL cell lines (JVM2, Jeko-1, G519, Z-138, Mino, and Maver) were maintained in RPMI-1640 medium (Gibco, 61870036) supplemented with 10% FBS and 1X Penicillin-Streptomycin (PS) (Gibco: 15140122). The mouse stromal cell line MS5 was obtained from Dr. C.P Chaturvedi, SGPGI, Lucknow, was maintained in αMEM (Sigma Aldrich, M0450) containing 10% FBS, 1 X PS and supplemented with Sodium Bicarbonate (ThermoFisher, 25080094). MS5 cells were passaged every 3-6 days by trypsinization using TrypLE (Gibco, 12605-028). For primary MCL/MS5 co-culture, MCL cells were plated on a pre-established confluent layer of MS5 cells in αMEM media and maintained at 37°C in a 5% CO_2 incubator. Once a week, MCL cells were either passaged to a new pre-established layer of MS5 cells, or culture populations were halved by carefully replacing half of the culture medium with fresh αMEM media. MCL cells adhered to MS5 cells were delicately dislodged through a phosphate buffer saline (PBS) wash procedure, succeeded by a brief trypsinization with TrypLE. This trypsinization protocol was tailored to facilitate the detachment of adherent MCL cells while ensuring the retention of MS5 cells, thus circumventing their inadvertent removal. Following this step, for experiments necessitating adherent MCL cells, any residual MS5 cells were eliminated from the MS5/MCL mixture post-trypsinization by transferring the mix onto a fresh 12-well plate. It is noteworthy that MS5 cells possess comparatively stronger adhesive properties than MCL cells, warranting this additional purification step to isolate the adherent MCL cell population effectively. All cell lines were cultured in mycoplasma-free conditions, and their identification was confirmed by short tandem repeat analysis. The BTK inhibitor ibrutinib (PCI-32765), FGFR1 inhibitor Erdafitinib (S8401), Bortezomib (PS-341), Doxorubicin (S1208), and Pirtobrutinib (LOXO-305) were purchased from Selleck Chemicals. Nucleolin targeting pseudopeptide N6L was kindly provided by Prof. José Courty (Université Paris-Est Créteil, France). Ibrutinib-resistant (Ibr-Res) MCL cells (Jeko-1 and Mino) were generated from parental-sensitive cells by perpetually cultured with incremental doses of ibrutinib.

Cloning and tetracycline-inducible expression of lentiviral-based CERS6-AS1 shRNA

Lentiviral tetracycline-based inducible shRNA for CERS6-AS1 (sh1-CERS6-AS1 and sh2-CERS6-AS1) were cloned in pLKO.1 plasmid. Lentivirus were generated by co-transfection of HEK293T cells with shRNA construct and Addgene packaging plasmids pMD.2G (12259) and psPAX2 (12260). MCL cells after transduction were selected with puromycin (1.0µg/mL) (Gibco, A1113803) for stable cell line generation and maintained in 10% tetracycline negative FBS (Himedia, RM10686) containing RPMI media. Expression of shRNA was induced by treating cells with doxycycline (5.0µg/mL) for seven days, lysed for immunoblots with RIPA buffer, and probed for indicated antibodies.

Cell viability, cell cycle, and apoptosis assay

Metabolic activity assay was performed using a WST-1 cell proliferation assay kit (MK400, Takara Bio) according to the manufacturer’s instructions. In each experiment, 10,000 cells were seeded in a well of 96 well plate in triplicates and treated for 72 hours with respective drugs.

DMSO-treated cells were used as the control. 10µL of WST-1 solution was added in each well, followed by 4 hours of incubation at 37ºC, 5% CO_2 incubator. Average absorbance was measured at 450 using a spectrophotometer (Victor3; PerkinElmer). Percentage survival was calculated by normalizing the OD of DMSO-treated cells with drug-treated cells, and the IC50 value was determined using GraphPad Prism 8.0 software. The combination index (CI) between the two drugs was calculated using CompuSyn software, and CI values < 0.9 were considered synergistic effects.

For cell cycle analysis, MCL cells were pelleted after the mentioned treatment and stained with propidium iodide (PI) (Sigma Aldrich, P4170). Samples were acquired using Flow Cytometry (BD Bioscience; FACSAria™ III, USA), and the percentage of cells in the cell cycle's G0, G1, S, and G2 phases were determined using FlowJo-V8 software.

For apoptosis assay, cells, after the respective drug treatment for the indicated time, were stained with Annexin V-FITC and PI staining kit as per the manufacturer's instructions (BD Bioscience; 556547). Data were acquired using Flow Cytometry (BD Bioscience, FACSAria™ III, USA), and the percentage of cells in early, late, and necrotic stages was determined using FlowJo-V8 software. To visualize necrotic/dead cells in primary MCL cells treated with respective drugs in the MCL/MS5 co-culture model, total MCL cells, including adhered and suspension population, were harvested and stained with 7-amino actinomycin D (7-AAD) (BD Bioscience, 559925). Cells were kept in the dark on ice before the analysis through flow cytometry.

Colony formation assay

A colony formation assay was performed using a methylcellulose medium (H4100; STEMCELL Technologies) as described previously. Briefly, cells were mixed with methylcellulose containing 20% FBS and 40% IMDM media and poured into a 35-mm plate using a 16-gauge needle. The colonies were allowed to grow for 7 days, stained with p-iodonitrotetrazolium violet (MP Biomedical, 102066) and imaged using a ChemiDOC imaging system (BoRad, 1708280SP)

ALDH1 activity assay

ALDH1 cell activity assessment was conducted employing an ALDEFLUOR kit sourced from STEMCELL Technologies (01700), following the manufacturer's prescribed protocol. In brief, following the respective treatments, cells were subjected to PBS (pH 7.5) washes and resuspended in 1 mL of ALDH1 buffer along with 5 µL of ALDEFLOUR reagent. Diethylaminobenzaldehyde (DEAB), a potent inhibitor of the ALDH1 enzyme, served as the reference control. Specifically, 5 µL of DEAB was promptly added to half of the cells (500 µL) contained in a separate Eppendorf tube for control purposes. The samples were subsequently incubated at 37°C in a 5% CO_2 environment for a duration of 45 minutes. Cell acquisition was performed utilizing the FL1 channel of the BD FACSLyric™ flow cytometer, with subsequent data analysis accomplished through the utilization of FlowJo-V8 software.

Immunoblotting

For immunoblotting analysis, both MCL cell lines and primary samples underwent washing with ice-cold PBS, followed by lysis in cold RIPA lysis buffer supplemented with Halt protease and phosphatase inhibitor (ThermoFisher, 87786). Subsequently, the total protein content was quantified utilizing the Pierce BCA Protein Assay Kit (ThermoFisher, 23227). Equal quantities of proteins were then resolved through sodium dodecyl sulfate-polyacrylamide gel electrophoresis and subsequently transferred onto PVDF membranes (BioRad, 1620177). The membranes were blocked utilizing 5% Blotting-Grade Blocker (BioRad, 12010020) and then subjected to incubation with various primary antibodies, followed by corresponding horseradish peroxidase-conjugated secondary antibodies. The immunoblots were visualized using SuperSignal™ West Pico PLUS Chemiluminescent Substrate (ThermoFisher, 34580) or West Femto Maximum Sensitivity Substrate (34095) in a ChemiDoc Imaging system (BioRad, 1708280SP). Densitometric analysis of the blots was performed utilizing ImageJ software. The specific human antigen-targeting antibodies, along with their respective catalogue numbers utilized in this study, are detailed below.

Antibodies	**Company**	**Catalog**	**Dilution**
Mouse monoclonal, β-Actin-HRP	Sigma Aldrich	A3854	1:10000
Rabbit monoclonal, β-Catenin	CST	D10A8	1:1000
Rabbit monoclonal, β-Catenin (Non-P active)	CST	D2U8Y	1:1000
Rabbit monoclonal, CDKN1C	ABclonal	A6843	1:1000
Rabbit monoclonal, c-Myc	CST	D84C12	1:1000
Rabbit monoclonal, Cyclin D1	CST	92G2	1:1000
Rabbit monoclonal, Ezh2	CST	D2C9	1:1000
Rabbit monoclonal, FGFR1	CST	D8E4	1:1000
Rabbit monoclonal, Nucleolin	CST	D4C70	1:1000
Rabbit monoclonal, pErk1/2	CST	D13.14.4E	1:1000
Rabbit monoclonal, pGSK-3β	CST	D85E12	1:1000
Rabbit monoclonal, pRb	CST	9308	1:1000
Rabbit monoclonal, Erk1/2	CST	137F5	1:1000
Rabbit monoclonal, GSK-3β	CST	D5C5Z	1:1000

CST: Cell Signaling Technology

Quantitative Real-time polymerase chain reaction (qRT-PCR)

Total RNA extraction from MCL cell lines, fresh MCL tumor, or formalin-fixed paraffin-embedded (FFPE) samples was carried out utilizing the Qiagen RNeasy Kit (74104) or the RNeasy FFPE Kit (73504) following the manufacturer's protocol. Subsequently, first-strand cDNA synthesis was performed using the Superscript III reverse transcriptase kit (BioRad, 1708891) in accordance with the manufacturer's instructions. qRT-PCR was conducted on the Applied Biosystems™ 7500 Real-Time PCR Systems (ThermoFisher, 4351106) utilizing SYBR Green PCR Master Mix and gene-specific primers. Normalization of all samples was accomplished using the internal loading control gene GAPDH, with results presented as relative fold changes between control and experimental groups.

Cytoplasmic and nuclear RNA extraction was conducted to identify the abundance of long non-coding RNA CERS-AS1. Briefly, cells were lysed with 0.25x cell lysis buffer comprising 50 mM Tris-Cl (pH 8), 100 mM NaCl, 5 mM MgCl2, and 0.5% NP-40, using a recommended volume of 300µL per sample. The lysate was kept on ice for 2 minutes with gentle vortexing every 45 seconds. The lysate was then centrifuged at 12,000 g at 4°C for 2 minutes. The cytoplasmic fraction was collected into a new tube, and the pellet was washed with 1x ice-cold PBS and centrifuged at 2,000 g for 5 minutes. RNA purification kit (Qiagen, 74104) was used for RNA extraction from separated nuclear and cytoplasmic fractions as per recommended kit protocol.

RNA stability assay

To determine RNA half-life, MCL cells were treated with actinomycin D (5µg/mL) (Sigma Aldrich, A1410) added to the culture media for specific time points (0, 3, and 6 hours). Subsequently, total RNA was extracted, converted into cDNA, and subjected to RT-PCR analysis. The cycle threshold (CT) value of each transcript was normalized to either 18S or β-actin RNA levels. Utilizing GraphPad Prism 8.0 software, RNA decay curves were generated based on the normalized CT values to elucidate the RNA half-life dynamics.

RNA Immunoprecipitation Assay (RIP)

A RIP (RNA Immunoprecipitation) assay was conducted to elucidate the interaction between the RNA binding protein nucleolin and the long non-coding RNA CERS-AS1 or FGFR1 mRNA. In brief, cells were lysed in ice-cold Polysome extraction buffer (PEB) comprising 20mM Tris-HCl (pH 7.5), 100mM KCl, 5mM MgCl2, and 0.5% Nonidet P-40, supplemented with RNase inhibitors (ThermoFisher, EO0381) and protease inhibitors (ThermoFisher, 87786). The lysate was then cleared by centrifugation at maximum speed. Prior to immunoprecipitation, nucleolin antibody (5µg, Sc-55486) or mouse IgG-control (5µg, Sc-2025), diluted in NT2 buffer (comprising 50mM Tris-HCl, pH 7.5, 150mM NaCl, 1mM MgCl2, and 0.05% Nonidet P-40), were allowed to bind overnight on a rotator at 4°C with magnetic beads (Pierce™ Protein A/G, 88802). Subsequently, the cleared lysates were incubated with the antibody-coated beads for 2 hours at 4°C with rotation, while 10% of the input was reserved for further analysis. The beads were washed five times with NT2 buffer, after which 30% of the beads were boiled with SDS loading dye for immunoprecipitated protein analysis. The remaining 70% of the beads were subjected to treatment with 2µL of DNAase (Qiagen, 79254) for 10 minutes at 37°C, followed by Proteinase K (Qiagen, RP-107P1) treatment, before RNA extraction with Trizol (Ambion, 15596026) according to the manufacturer's instructions. The isolated RNA was reverse transcribed, and qRT-PCR was performed as previously described to analyze the interaction between nucleolin and the target RNAs.

Immunophenotyping

Following the respective treatment, MCL cell lines or primary MCL were pelleted and washed once with PBS, then blocked using FACS blocking buffer containing 2% FBS and 2mM EDTA (Invitrogen, AM9260G) for 30 minutes on ice to minimize nonspecific binding. Cells were stained using human antigen-specific fluorochrome-labeled antibodies from BD Biosciences:

CD44-FITC (560977), CD45-FITC (560976), CD19-PE (555413), CD20-FITC (555622) on ice for 30 minutes before acquisition at BD FACSLyric™.

Analysis of RNA-protein interactions

To predict the interaction of CERS6-AS1 lncRNA and FGFR1 mRNA, we screened the entire human proteome database using *catRAPID omics v2*. Sequences of complete RNA were used as input to *catRAPID omics v2* to identify potential protein interactors. This provided details on potential protein interactors and the specific regions of the input mRNA that interact with stretches of the target protein structure. The results were further validated by a second screening. This time, only the identified stretches of the RNA (CERS6-AS1 or FGFR1 mRNA) sequences from the previous step were used as input along with the complete sequence of nucleolin to validate the potential binding region of nucleolin protein. This additional screening confirmed the identification of nucleolin as an interactor for both CERS6-AS1 and FGFR1 mRNA.

Prediction of G-triplex motif and classification of classifies G-quadruplex-RNA binders

Prediction of G-quadruplex region in the sequence of CERS6-AS1 RNA sequence was performed through G4 Hunter. The region of maximum interaction propensity, as predicted by *catRAPID omics v2.0*, were used as query sequence for the prediction. The predictors identified the potential G-quadruplex structures within the given sequences. To determine the type of G-quadruplex that preferentially binds to nucleolin protein, we used the G4-Folded/UNfolded Nuclear Interaction Explorer System (G4-FUNNIES) tool for estimating RNA G4-binding propensities. This algorithm was developed through training to distinguish between nuclear proteins that bind to folded G4 structures and those that bind to unfolded G4 structures. By analysing protein binding in these different environments (rich in potassium (K+), sodium (Na+), or lithium (Li+) etc), G4 FUNNIES precisely identifies and classifies G-quadruplex-RNA binders.

Structure modelling

The modelling of G-triplex motif structure of CERS6-AS1, as well as of stem loop structure of FGFR1 interacting motifs, was performed with recent released package Alphafold 3. The three-dimensional structure of nucleolin complex particularly the RNA binding domains (RBD) propensities (RBD1,2,3 and 4) with the G-triplex motif of CERS6-AS1 and the identified interacting motif of FGFR1 mRNA were also modelled through Alphafold-3.

Results:

Elevated CERS6-AS1 expression is associated with poor survival in MCL patients

Over the past three years, investigations have highlighted the potential oncogenic role of novel lncRNA CERS6-AS1 in various solid cancers (26). To elucidate the expression pattern of CERS6-AS1 in MCL, we examined blood samples from patients in leukemic phase, lymph node biopsies and FFPE tumors obtained from chemo-naive MCL patients (n=98). As a comparative control, we have isolated PBMCs and total B-cells ($CD19^{+}$) from age related healthy donors (n=12) and observed a significantly elevated expression of CERS6-AS1 in MCL (Fig. 1A).

Besides MCL, CD5 is also expressed on a subset of normal naive B cells, which can lead to some similarities in characteristics between CD5-positive naive B cells and MCL cells. Therefore, we have isolated naïve B-cell subsets ($CD3^{-}CD45^{+}CD19^{+}CD5^{+}$) from healthy donor's peripheral blood (n=13) and compared CERS6-AS1 expression. We found a significant expression of CERS6-AS1 in MCL compared to naïve B-cells. We divided MCL cohort into high or low CERS6-AS1 expressing groups, where the top 33% and bottom 33% of tumors from normalized (median ddCT) value were considered as high and low CERS6-AS1 expressing tumors respectively. Subsequently, we analyzed the association between CERS6-AS1 expression and clinicopathologic characteristics in a subset of patients with available clinical information (n=54).

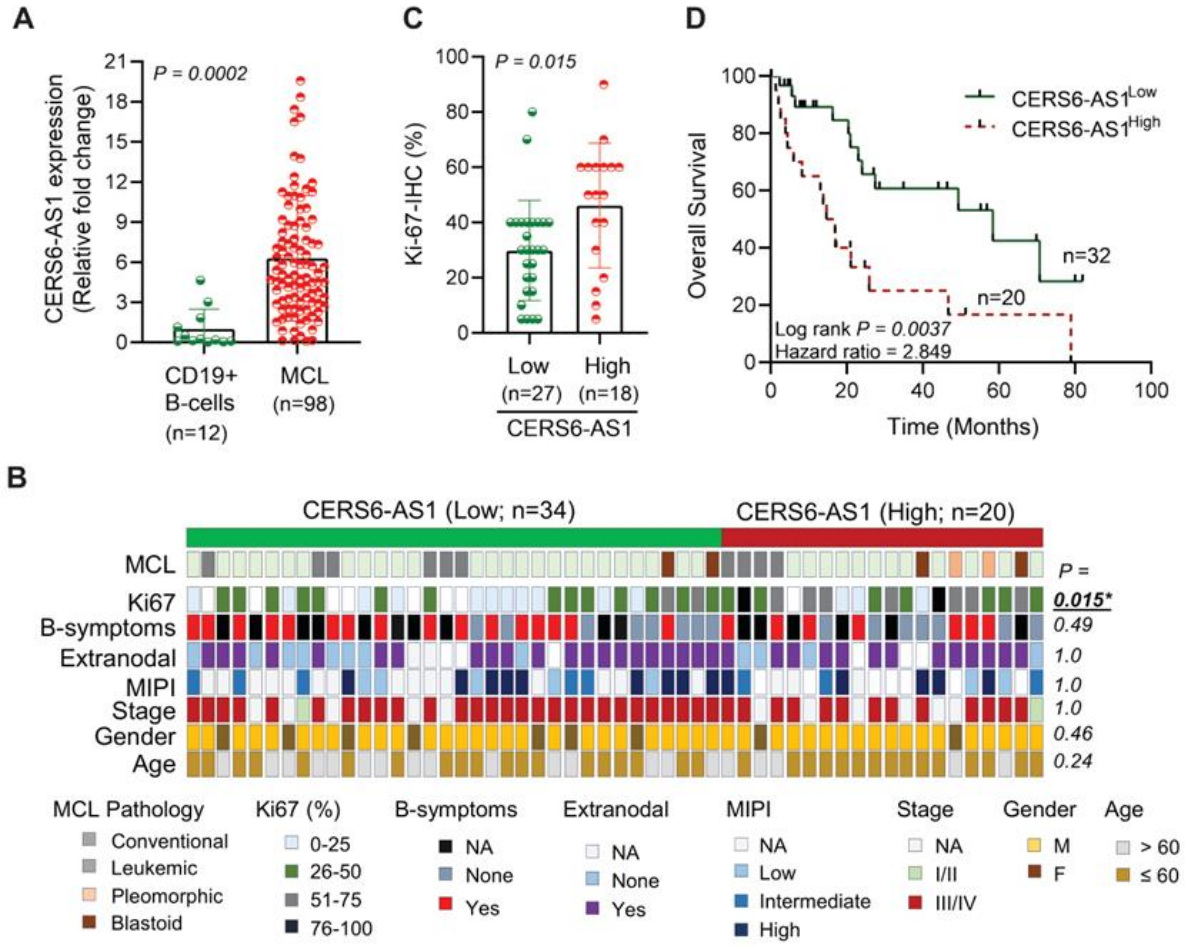

Fig. 1 Elevated CERS6-AS1 expression is associated with poor survival in MCL Patients. (A) CERS6-AS1 expression was assessed by qRT-PCR in CD19+ B-cells from healthy donors (n=12) and MCL tumor samples (n=98). Statistical analysis was performed using two tallied unpaired Student's t-test. **(B)** Clinical characteristics were compared between high (n=20) and low (n=32) CERS6-AS1 expressing MCL groups (Fisher's exact test). **(C)** Positive correlation of CERS6-AS1 expression with proliferation marker Ki-67 in primary MCL. *P = 0.015*, two-tailed, unpaired Student's t-test. **(D)** A Kaplan-Meier plot of

overall survival was generated and analyzed with the Log-rank Mantel-Cox test *(P = 0.0037)* for MCL patients, showing that the high CERS6-AS1 expression is associated with poor outcomes.

Though there were not significant correlations (Fisher's exact test) between CERS6-AS1 expression and clinical characteristics, including extra nodal involvement, B-symptoms, disease stage, clinicopathologic subtypes (classic, blastoid, and leukemic), and Mantle Cell Lymphoma International Prognostic Index (MIPI) score observed (Fig. 1B. However, immunohistochemical staining data for Ki-67 revealed a significantly higher proportion of Ki-67 positive cells in CERS6-AS1^{High} group compared to the CERS6-AS1^{Low} expressing group (*P=0.015*) (Fig. 1C). Kaplan–Meier analyses demonstrated a significant association, where high CERS6-AS1 expressing groups had poor overall survival in MCL patients (Mantel-Cox Log-rank, *P=0.0037*) (Fig. 1D). These findings underscore the potential prognostic significance of CERS6-AS1 expression in MCL.

CERS6-AS1 expression is positively correlated with cancer stem cell characteristics

Previous studies have underscored the significant impact of physical interaction between MCL and stromal cells, demonstrating enhanced survival benefits and drug resistance acquisition (11). In this context, we conducted experiments wherein patient-derived MCL cells (n=6) were cultured on a confluent layer of mouse stromal cells (MS5) and explored its influence on MCL cell viability and drug resistance. Our findings revealed a notable increase in MCL cell proliferation and a concomitant loss of response to FDA-approved BTK inhibitors, including both covalent (Ibrutinib) and non-covalent inhibitors (Pirtobrutinib, LOXO-305;). Intriguingly, we also observed a significant upregulation in the expression of cancer stem cell signature genes, (CD44 and Nanog), in the MS5 co-cultured MCL cells. Next, we assessed the expression of CERS6-AS1 in mono-cultured and MS5 co-cultured patient-derived MCL, and in MCL cell lines (Jeko-1 and Mino). Our analyses revealed a significant elevation in CERS6-AS1 expression in co-cultured MCLs compared to mono-cultured ones (Fig. 2A-B). In our MS5/MCL co-culture, we observed a heterogeneous MCL population, wherein a subset of MCLs (near to 10%) adhered to stromal cell layer while remaining cells grew in suspension. Based on prior studies, these adherent MCL cells exhibit cobblestone-area forming characteristics and demonstrated an upregulation of canonical and non-canonical nuclear factor κB (NF-κB) signaling (11, 15, 35). To separate out the adherent MCL population from MS5 layer, we employed a slow trypsinization process, which allowed the detachment of MCL cells only without detaching stromal cell adhered layer. Flow cytometry analysis confirmed the purity of separated adherent MCL cells, which displayed high CD45 expression which is present on almost all hematopoietic cells but is absent on MS5 cells. We further noticed these adherent MCLs express a low level of pan B-cell marker CD19 compared to MCLs in suspension, and none of these populations were positive for hematopoietic stem cell marker CD34 or T-cell marker CD3, suggesting that our cultured patient-derived leukemic MCL had predominantly malignant B-cell population. Subsequent analysis of separated adherent and suspension MCL cells from MS5/MCL co-cultured population revealed a significant increase in expression of CERS6-AS1, and stem cell markers CD44, and Nanog in adherent MCLs compared to suspension ones (Fig. 2C). Notably, adherent MCL cells exhibited a reduced sensitivity to BTK inhibitors. Given that adherent MCL cells express low levels of CD19 and higher levels of cancer stem cell markers, we examined these characteristics in total leukemic MCL without co-culturing with stromal cells. Specifically, we

FACS-sorted $CD3^{-}CD34^{-}CD45^{+}CD19^{low}$ and $CD3^{-}CD34^{-}CD45^{+}CD19^{high}$ MCL population from the peripheral blood of leukemic stage of MCLs (n=10). Note: prior study from Mathur *et al* had demonstrated these $CD45^{+}CD19^{low}$ cells have tumor initiating properties (5). Consistent with findings from adherent MCL cells, $CD45^{+}CD19^{low}$ cells exhibited high CERS6-AS1 expression and demonstrated reduced sensitivity to chemotherapeutic agents (Fig. 2D).

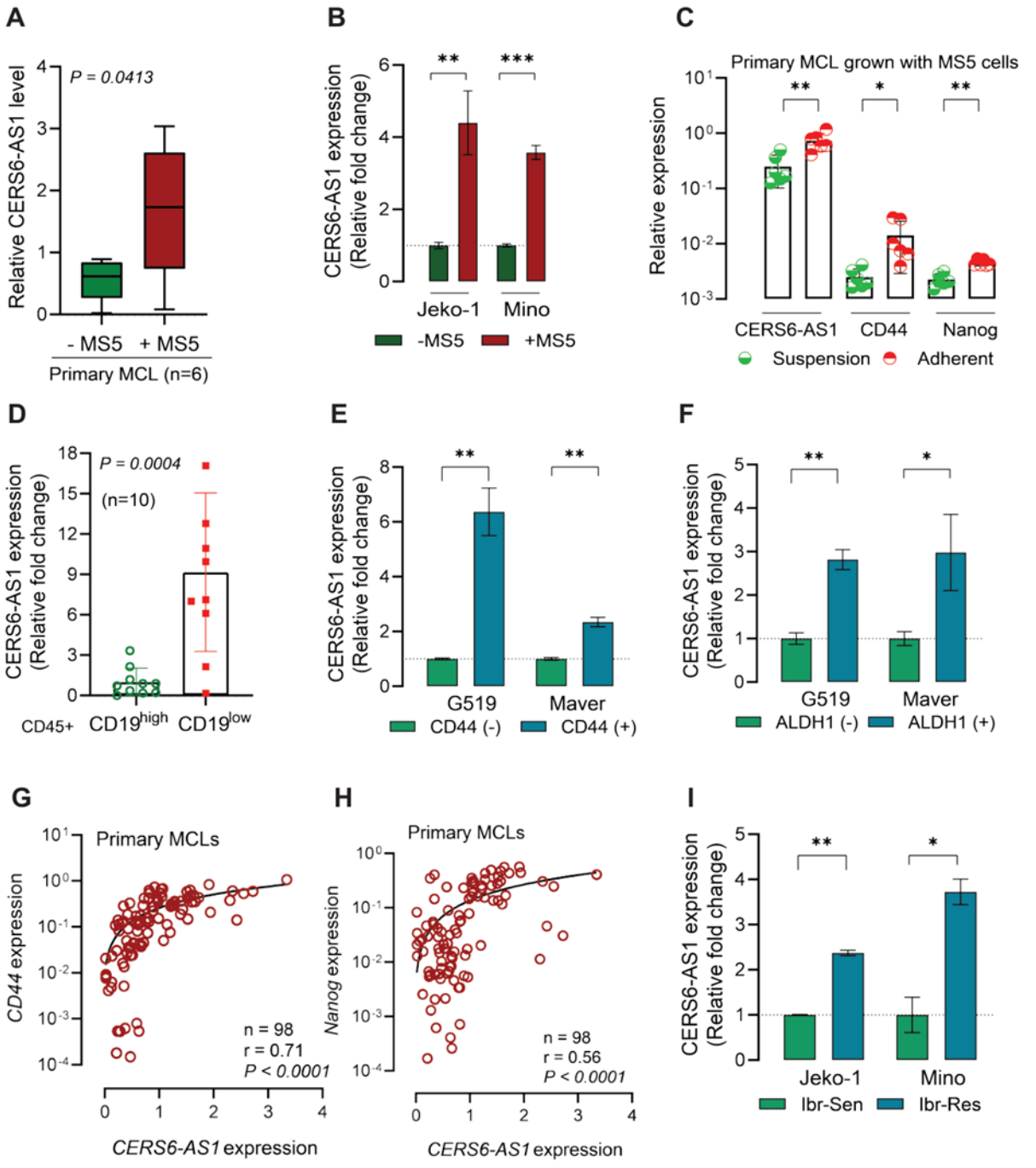

Fig. 2 CERS6-AS1 expression and its correlation with cancer stem cell characteristics. (A) Expression of CERS6-AS1 in primary MCL (n=6) grown under *in vitro* condition without or with mouse

stromal cells (MS5) assessed by qRT-PCR. Note: we do not observe significant changes in our endogenous control gene GAPDH level when co-cultured with MS5 cells. **(B)** Expression of CERS6-AS1 in MCL cell lines (Jeko-1 and Mino) was increased when cells were co-cultured with MS5 cells relative to mono-cultured cells (dotted line). **(C)** Elevated expression of CERS6-AS1 and stem cell markers CD44 and Nanog in primary MCL cells (n=6) those adhered to MS5 cells than in suspension cells co-cultured with MS5 cells. **(D)** Higher expression of CERS6-AS1 in $CD45^{+}CD19^{low}$ than $CD45^{+}CD19^{high}$ primary MCL cells, isolated by FACS sorting from MCL patient blood with leukemic stage (n=10). **(E)** MCL cell lines (G519 and Maver) were FACS sorted for CD44 (+) and CD44 (-) populations, where CD44 (+) cells showed elevated CERS6-AS1 expression compared to CD44 (-) cells (dotted line). **(F)** Similar to CD44 (+) MCL cell, the ALDH1 (+) population by FACS sorting has a higher CERS6-AS1 level than ALDH1 (-) cells (dotted line). **(G, H)** Correlation plot between CD44 and CERS6-AS1 expression or Nanog and CERS6-AS1 in primary MCL (n=98); Pearson correlation, two tailed $P < 0.0001$. Data showing a positive correlation of CERS6-AS1 expression with the expression of stem cell markers level. **(I)** CERS6-AS1 expression by qRT-PCR in BTK inhibitor-resistant MCL cell lines (Jeko-1 and Mino) generated by culturing parental sensitivity in the presence of increasing doses of ibrutinib as described in method. Each bar represented mean ± SD of three independent experiments. Groups were compared by two tailed unpaired Student's t-test; *$P < 0.05$, **$P < 0.01$, or ***$P < 0.001$

To further validate the association between CERS6-AS1 expression and cancer stem cell markers, we performed FACS sorting in MCL cell lines (G519 and Maver) and isolated CD44 (+) and CD44 (-) cells. As anticipated, CD44 (+) cells displayed higher CERS6-AS1 expression (Fig. 2E). This signature was further corroborated using another cancer stem cell marker, ALDH1, wherein ALDH1 (+) cells exhibited higher CERS6-AS1 levels compared to ALDH1 (-) cells (Fig. 2F). Additionally, correlation analysis conducted in total primary MCL (n=98) unveiled a positive correlation between CERS6-AS1 and CD44 ($P < 0.0001$; r = 0.71) as well as Nanog expression ($P < 0.0001$; r = 0.56) (Fig. 2G-H). As adherent MCL cells displayed resistance to BTK inhibitors, we established ibrutinib-resistant MCL model (Jeko-1 and Mino) by subjecting them to escalating doses of ibrutinib in culture media. WST-1 experiments confirmed the development of ibrutinib resistance, with significantly higher expression levels of CERS6-AS1 observed in resistant cells (Fig. 2I).

Downregulation of CERS6-AS1 reduces cancer stem cell signatures and sensitizes MCL cells to BTK inhibitor

To investigate the functional significance of CERS6-AS1, we first analyzed its basal level in six MCL-derived cell lines which revealed variable expression of CERS6-AS1, with the highest expression was observed in JVM2, followed by Mino and Maver and least expression was in Z-138. We further performed qRT-PCR from isolated nuclear and cytoplasmic fractions which revealed a significant cytoplasmic localization of CERS6-AS1 in MCL cell lines (Fig 3A). Note: stable CERS6-AS1 knockdown was not achieved in JVM2 as cells did not survive. Therefore, we generated tetracycline-inducible stable knockdown clones in Mino and Maver cell lines using two different CERS6-AS1 targeting shRNAs. Approximately 80% of CERS6-AS1 knockdown was achieved with both shRNA that led to notable alterations in cell cycle progression, with a significant increase in proportion of cells in G0/G1 phase and a decrease in S and G2M phases (Fig. 3B). Furthermore, a significant reduction in the expression of cancer stem cell markers (Oct4, CD44, Myc, and Nanog), was observed consistently in both shRNA knockdown clones (Fig. 3C).

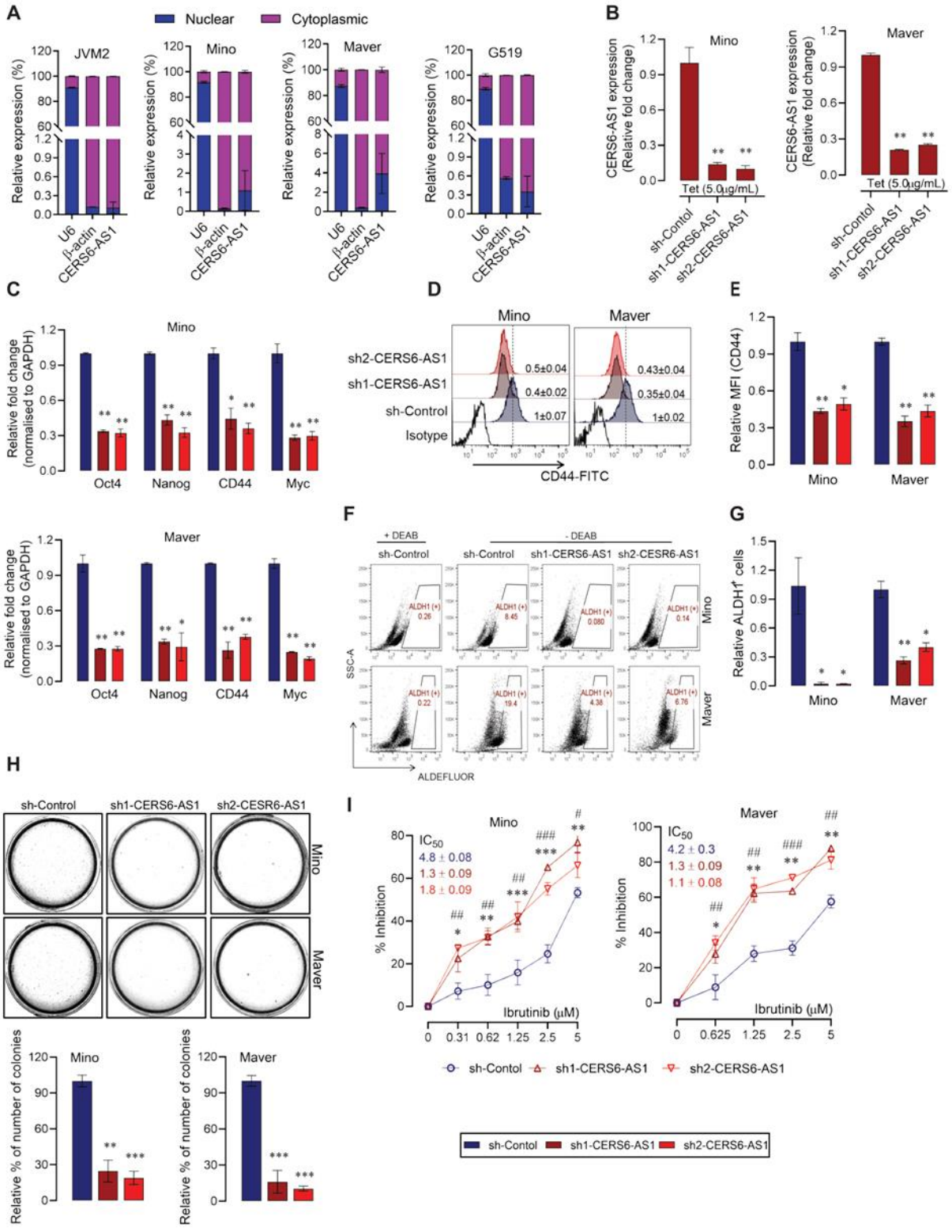

Fig. 3 CERS6-AS1 downregulation inhibits cancer stem cell marker expression and sensitizes MCL cells to chemotherapeutic agents. (A) Relative CERS6-AS1 expression in nucleus and cytoplasm fractions by qRT-PCR in MCL cell lines (n=4). U6 and β-actin were used to serve as the internal reference

of nucleus and cytoplasmic fractions respectively. (**B)** Tetracycline inducible stable knockdown of CERS6-AS1 expression in MCL cells (Mino and Maver) by qRT-PCR using two different CERS6-AS1-specific shRNAs. Tetracycline was added twice (day 0 and day 3) at a concentration of 5µg/mL. Cells were harvested at day 7 for further experiments. **(C)** Expression of stem cell markers (CD44, Nanog, Oct4, and Myc) were downregulated in CERS6-AS1 knockdown MCL cells assessed by qRT-PCR. **(D)** Expression of cell-surface CD44 level in sh-Control and CERS6-AS1 knockdown cells by flow cytometry and quantification showed relative mean fluorescence intensity (MFI) **(E)**. **(F)** ALDH1 activity in CERS6-AS1 knockdown MCL cells using ALDEFLUOR kit and respective quantification shown as relative $ALDH1^+$ cells **(G)**. **(H)** Colony formation assay was performed CERS6-AS1 knockdown groups compared to sh-Control MCL. Quantification of colonies in sh-Control and CERS-AS1 knockdown cells. **(I)** WST-1 cell metabolic activity assay was performed in CERS6-AS1 knockdown and sh-Control MCL cells after 72 hours of treatment with BTK inhibitor at indicated concentrations. CERS6-AS1 knockdown cells showed reduced cell survival (* denoted comparison between sh-Control vs sh1-CERS6-AS1; and # denoted comparison between sh-Control vs sh2-CERS6-AS1 groups). Each bar represented mean ± SD of three independent experiments. Groups were compared by two tailed unpaired Student's t-test; *$P < 0.05$, **$P < 0.01$, or ***$P < 0.001$*

We further tested the surface level of CD44, where CERS6-AS1 knockdown resulted in a decrease in surface CD44 expression, a hallmark of cancer stem cells (Fig. 3D-E). Additionally, a reduction in the population of ALDH1+ cells was observed in CERS6-AS1 knockdown cells, corroborating the role of CERS6-AS1 in maintaining cancer stem cell characteristics in MCL (Fig. 3F-G). We performed colony formation assays which demonstrated fewer colonies in methylcellulose matrix in CERS6-AS1 knockdown cells compared to respective controls, indicating a decrease in clonogenic potential, a characteristic feature of cancer stem cells (Fig. 3H). Importantly, CERS6-AS1 knockdown cells exhibited increased sensitivity to BTK inhibitor, as evidenced by a significant increase in growth inhibition compared to control cells (Fig 3I). Our findings, validated in multiple sets of experiments, suggest that CERS6-AS1 is upregulated in MCL and plays a critical role in promoting cancer stem cell characteristics and chemotherapy resistance. Depletion of CERS6-AS1 expression attenuated these stem cell signatures and enhances sensitivity to chemotherapeutic agents, highlighting its potential role as a therapeutic target in MCL.

CERS6-AS1 expression is positively correlated to FGFR1 expression in MCL

CERS6-AS1 has shown its oncogenic activity in various solid tumors by modulating the expression of genes including SPTBN2, FGFR1, HMGA1, YWHAG and BAP (26). Among these, FGFRs are pivotal members of receptor tyrosine kinase family, with its aberrant activation and promotion of stem cell-like signatures has been frequently observed in various cancers (36-40). Given these associations, we sought to investigate the significance of FGFR axis in MCL. In our study, we initially assessed the expression of FGFR isoforms in primary MCL samples (n=76) which revealed a notably higher expression of FGFR1 compared to FGFR2 and FGFR3. Further exploration of FGFR expression in patient-derived MCL cells (n=6) in mono-cultured and MS5 co-cultured MCLs, demonstrated consistent upregulation of FGFR1 in co-cultured condition (Fig. 4A). Similar to CERS6-AS1, FGFR1 exhibited higher expression in primary MCL cells and cultured cell lines adhered to stromal layer compared to suspension-MCL cells (Fig. 4B-D). Like CERS6-AS1, FGFR1 expression was found to be elevated in FACS-sorted $CD3^-CD34^-CD45^+CD19^{low}$ MCL (having tumor initiating cell properties) compared to

$CD3^{-}CD34^{-}CD45+CD19^{high}$ MCLs (Fig. 4E). Correlation analysis conducted in total MCL (n=76) revealed a positive correlation between CERS6-AS1 and FGFR1 expression ($P < 0.0001$; r = 0.59), but not with FGFR2 or FGFR3 further supporting the notion of an association between the two genes (Fig. 4F). To explore potential regulatory relationship between CERS6-AS1 and FGFR1, we examined FGFR1 expression in CERS6-AS1 knockdown cells, where a significant downregulation of FGFR1 expression, both at RNA and protein was observed, indicating a potential regulatory role of CERS6-AS1 in modulating FGFR1 expression (Fig. 4G-H). Recent study has identified the oncogenic mechanism of FGFR1 in MCL where it regulates cell cycle progression via EZH2 which regulates Rb-E2F1 transactivation by CDKN1C (13). Consistent to this study, downregulation of FGFR1 expression in our CERS6-AS1 knockdown cells had abrogated oncogenic ERK1/2-EZH2-CDKN1C axis (Fig. 4I). Beside EZH2 associated cell cycle regulation, FGFR1 activation has also been linked to the upregulation of Wnt signaling leading to cancer stemness (41). We noted a significant downregulation of Wnt target genes in CERS6-AS1 knockdown cells where we have reduced FGFR1 expression further confirming abrogated cancer stem cell characteristics in these cells (Fig. 4J). In summary, our findings suggest that CERS6-AS1 may regulate FGFR1 expression in MCL, highlighting a potential mechanism by which CERS6-AS1 may contributes to harmonized FGFR signaling in MCL.

Nucleolin interacts with CERS6-AS1 and FGFR1 transcript and regulates their stability

LncRNAs exert their regulatory functions via interactions with RNA-binding proteins (RBPs) which act as scaffolds or guides RBPs to specific genomic loci or RNA transcripts, thereby modulating gene expression and functions (42). We found CERS6-AS1 knockdown cells have reduced FGFR1 expression in MCL. Therefore, we asked if CERS6-AS1 exerts its function via interacting with a RBPs. Using CERS6-AS1 RNA template, we screened for human proteome database using *catRAPID omics v2* and identified nucleolin as CERS6-AS1 interacting protein among the other proteins. We also carried out a bioinformatics analysis using the RNA-Protein Interaction Prediction tool (http://pridb.gdcb.iastate.edu/RPISeq/) that identified a prediction score of 0.75 and 0.97 using RF and SVM classifier respectively indicating that the CERS6-AS1 and nucleolin protein are likely interacting (43). Using *CatRAPID omics, we* further identified that nucleolin RBD (amino acid 307-647) interact with CERS6-AS1 regions spanning “986-1123” bases with the highest interactions propensities. Nucleolin preferably interacts with G-quaduplex regions of target RNAs. Therefore, we investigated whether CERS6-AS1 lncRNA contains any G-quadruplex/G-triplex motifs using G4 Hunter. Our results indicate that the region “1057-1079” bases (CCUAGGGGUGGGGAGGGGCCAGU) of CERS6-AS1 has high propensity for forming G-triplex motif. Further sequence analysis revealed that the region 1057-1079 bases contain three tracts of 4Gs, suggesting a likely adaptation of G-triplex topology. To further validate the interaction of CERS6-AS1, we modelled the CERS6-AS1:nucleolin complex structure using Alphafold3 that identified high propensity for interaction with nucleolin region RBD3 and RBD4 and exhibiting a greater number of non-covalent interactions (Fig 5A).

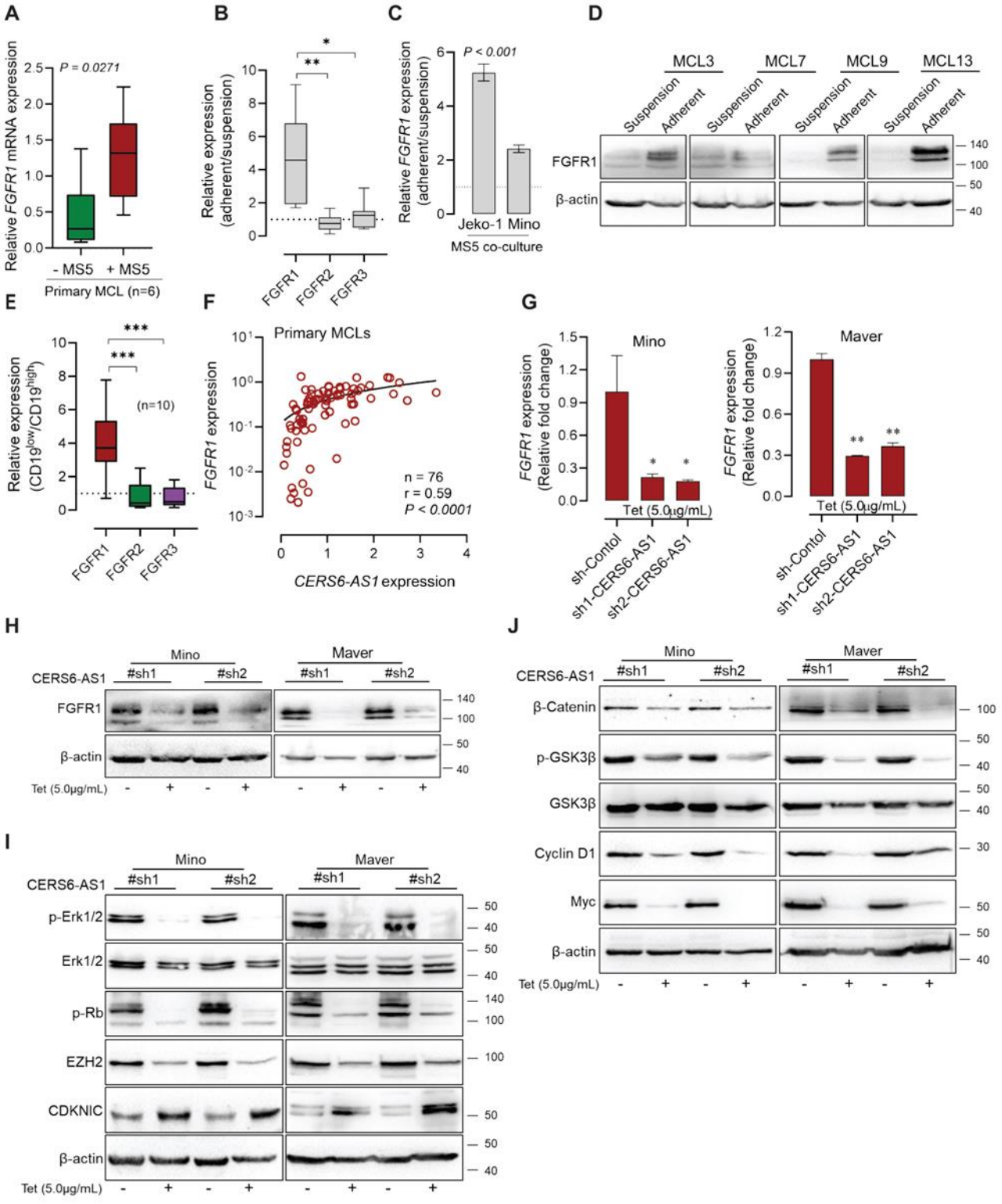

Fig. 4 Correlation between FGFR1 and CERS6-AS1 expression in MCL. (A) Expression of FGFR1 in primary MCL (n=6) grown *in vitro* condition without or with stromal cells (MS5) assessed by qRT-PCR. Elevated expression of FGFR1 in primary MCL cells (n=6) **(B)** and two MCL cell lines (Jeko-1 and Mino)

(C) those adhered to MS5 cells than in suspension in MCL/MS5 co-culture model. **(D)** Western blot analysis confirming elevated FGFR1 expression in primary MCL cells adhered to MS5 cells compared to those were grown in suspension. **(E)** Higher level of FGFR1 expression in $CD45^{+}CD19^{low}$ than $CD45^{+}CD19^{high}$ primary MCL cells isolated by FACS sorting from MCL patient blood with leukemic stage (n=10). **(F)** Correlation plot depicting the relationship between FGFR1 and CERS6-AS1 expression in primary MCL (n=76). Data showing a positive correlation of CERS6-AS1 expression with FGFR1; Pearson correlation, two tailed *P < 0.0001*. **(G)** Relative FGFR1 expression at RNA level (qRT-PCR) in sh-Control and CERS6-AS1 knockdown MCL cells (Mino and Maver). Significant downregulation of FGFR1 expression at protein level was observed in CERS6-AS1 knockdown cells **(H)**. **(I)** Western blot showing the expression of p-Erk1/2, p-Rb, EZH2, and CDKN1C upon CERS6-AS1 knockdown in 2 MCL cell lines. **(J)** Western blot showing the expression of Wnt signaling proteins: β-catenin, Myc, Cyclin D1 and p-GSK3β upon CERS6-AS1 knockdown in 2 MCL cell lines. Groups were compared by two tailed unpaired Student's t-test; **P < 0.05, **P < 0.01, or ***P < 0.001*

Nucleolin is a RBP that has been widely studied in hematological malignancies, have critical oncogenic functions by various mechanisms in multiple cancers, including lymphoma, and therefore considered as a potential anti-cancer target (44-47). We noticed a moderate but positive correlation between nucleolin and CERS6-AS1 expression in primary MCL ($P < 0.0231$; $r = 0.26$). In addition, we observed a significantly elevated level of nucleolin in primary MCL compared to $CD19^{+}$ B-cells from healthy donors(45) suggesting that nucleolin could have oncogenic functions in MCL. To further confirm the association between nucleolin:CERS6-AS1, we performed RNA immunoprecipitation (RIP) using nucleolin-specific antibody in MCL cell lines (Mino and Maver) those were prior treated with nucleolin-targeting nucant (N6L; 10.0μM) for a short period (2.0 hours) that did not alter MCL cells viability. Our findings revealed a specific binding of CERS6-AS1 to nucleolin, which was attenuated upon N6L treatment; 15 and 10.9-fold binding of CERS6-AS1 to nucleolin protein relative to IgG control, and that was reduced to 3.8 and 1.9-fold in N6L treated cells in Mino and Maver cell lines, respectively (Fig 5B-C). As CERS6-AS1 knockdown reduced FGFR1 expression in MCL. Therefore, we further explore if nucleolin and CERS6-AS1 form a complex with FGFR1 transcript and regulate its stability. We performed RNA immunoprecipitation (RIP) with a nucleolin antibody and found that FGFR1 transcript interacts with nucleolin, and this interaction is likely dependent on CERS6-AS1 as enrichment of FGFR1 transcript in the nucleolin-RIP complex was significantly reduced in CERS6-AS1 knockdown cells compared to controls (Fig. 5D-E). As of note: this decreased pull-down efficiency of FGFR1 transcript in CERS6-AS1 knockdown cells could be due to its lower FGFR1 availability. Therefore, considering this reduced basal level of FGFR1 expression in CERS6-AS1 knockdown, we have normalized the nucleolin-RIP-FGFR1 enrichment fraction with their respective endogenous basal expression (input samples). Nucleolin is known to interact with various RNA molecules, and by stabilizing oncogenic RNA, it regulates their oncogenic properties. To examine whether FGFR1 or CERS6-AS1 interaction with nucleolin in RIP complex could modulate their stability. Therefore, we performed an actinomycin D based RNA-chase experiments using control, CERS6-AS1 knockdown, and N6L-treated MCL cells. Where post 6 hours of actinomycin treatment led no significant changes in the fraction of CERS6-AS1 level between control and N6L treated group; whereas either CERS6-AS1 knockdown or N6L treatment significantly altered the half-life of FGFR1 transcript (normalized with basal input level) (Fig. 5F).

Subsequent investigation into the downstream effects of nucleolin inhibition by N6L revealed a significant downregulation of FGFR1 expression in MCL cell lines (n=6). Notably, while FGFR1 expression was consistently reduced, CERS6-AS1 expression showed marginal downregulation in a subset of MCL cells (Maver, Z-138, G519) (Fig. 5G). In line with the above observation, we found a positive correlation between nucleolin and FGFR1 expression ($P < 0.0001$; r = 0.57) in primary MCL (n=76) (Fig. 5H). These observations implying that beside via CERS6-AS1, there could be a direct association of nucleolin with FGFR1 transcript and therefore regulating FGFR1 transcript stability. Therefore, we performed an in-silico analysis using identical tools utilized for CERS6-AS1 and nucleolin interaction, and identified a direct interaction between nucleolin protein and FGFR1 transcript specifically the 5'UTR "538-573" bases region of FGFR1 mRNA predicted to forms a stem loop structure with a much higher propensity and interact strongly with nucleolin RBD1 and RBD2 respectively (Fig. 5I).

To further understand the impact of nucleolin on regulation of FGFR1 and CERS6-AS1 expression, using two nucleolin targeting shRNAs, we performed tetracycline-inducible-based stable nucleolin knockdown in Mino and Maver cell lines. Interestingly, we observed a significant downregulation of FGFR1 expression both at transcript and at protein level along with downregulation of FGFR1 target Myc expression (Fig. 5J). Interestingly, beside reduction in FGFR1 expression in nucleolin knockdown cells, we observed a significant downregulation of CERS6-AS1 expression and consequent reduction in cell viability when cells were kept longer with tetracycline containing media (96 hours) (Fig. 5K-L). This result implying that nucleolin expression in MCL potentiality regulating CERS6-AS1 expression or stability via other mechanism.

To assess the therapeutic potential of targeting nucleolin in MCL, we evaluated efficacy of N6L treatment in control and CERS6-AS1 knockdown cells. Similar to reduced viability of nucleolin knockdown MCL cells, N6L treatment inhibited cell growth and induced apoptosis, particularly in CERS6-AS1 knockdown cells having reduced FGFR1 expression, highlighting the importance of the nucleolin-CERS6-AS1-FGFR1 axis in MCL pathogenesis (Fig. 5M-N). We next evaluated nucleolin expression in primary MCL co-cultured with stromal cells. Unlike FGFR1 or CERS6-AS1, nucleolin expression was not altered in MCLs when co-cultured with stromal cells. Additional, examination of nucleolin expression in FACS sorted $CD3^{-}CD34^{-}CD45^{+}CD19^{low}$ and $CD3^{-}CD34^{-}CD45+CD19^{high}$ MCL; or in suspension vs adherent groups revealed no significant alterations in nucleolin expression. Moreover, nucleolin expression was also not altered in CERS6-AS1 knockdown cells suggesting that nucleolin levels present in these subsets of MCLs are sufficient to exert oncogenic functions.

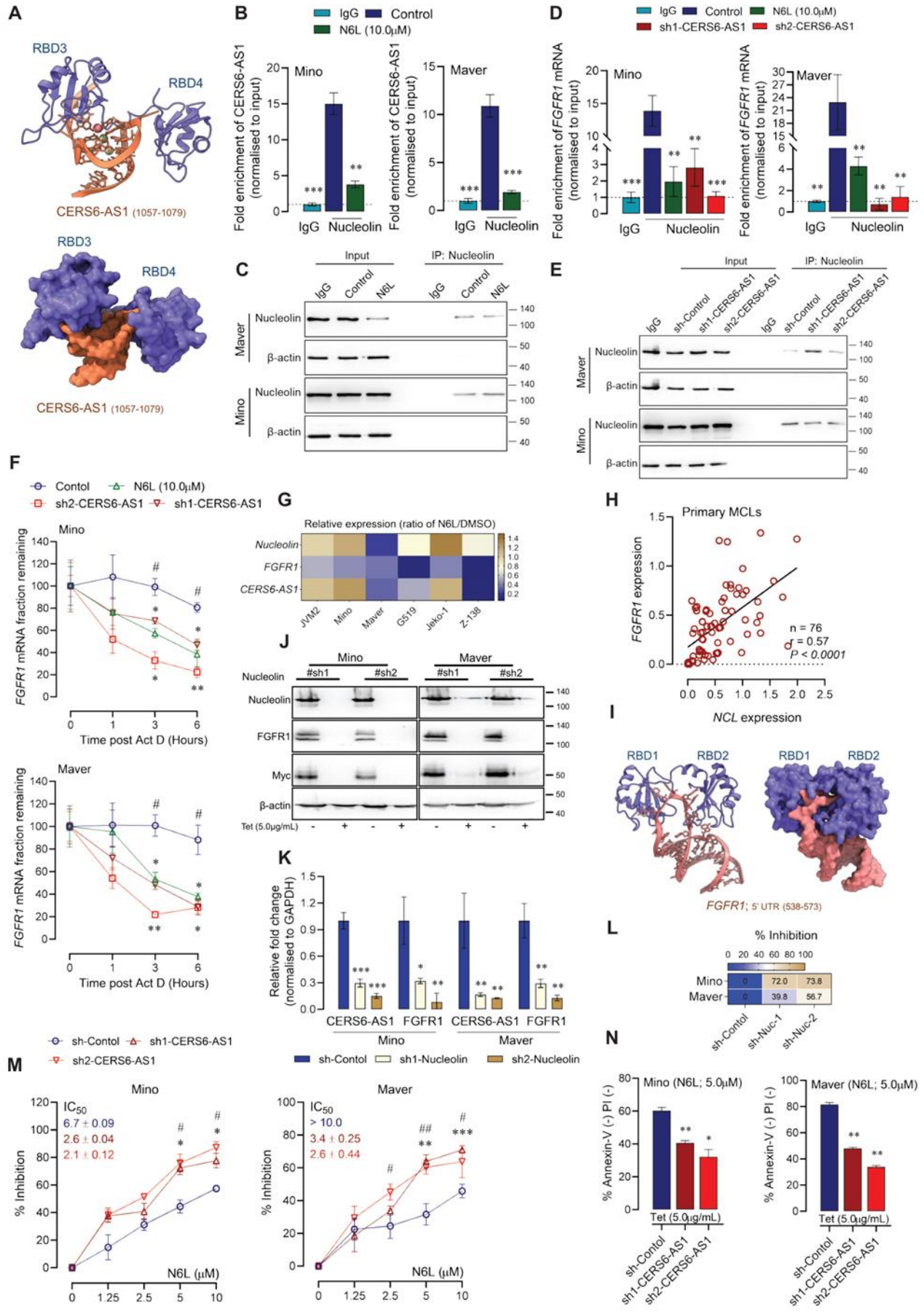
A
RBD3
RBD4
CERS6-AS1 (1057-1079)
RBD3
RBD4
CERS6-AS1 (1057-1079)
B
IgG
Control
N6L (10.0μM)
Mino
Maver
Fold enrichment of CERS6-AS1 (normalised to input)
IgG
Nucleolin
C
Input
IP: Nucleolin
IgG
Control
N6L
Maver
Mino
Nucleolin
β-actin
D
IgG
Control
N6L (10.0μM)
sh1-CERS6-AS1
sh2-CERS6-AS1
Mino
Maver
Fold enrichment of FGFR1 mRNA (normalised to input)
IgG
Nucleolin
E
Input
IP: Nucleolin
IgG
sh-Control
sh1-CERS6-AS1
sh2-CERS6-AS1
Maver
Mino
Nucleolin
β-actin
F
Contol
N6L (10.0μM)
sh2-CERS6-AS1
sh1-CERS6-AS1
Mino
Maver
FGFR1 mRNA fraction remaining
Time post Act D (Hours)
G
Relative expression (ratio of N6L/DMSO)
Nucleolin
FGFR1
CERS6-AS1
JVM2
Mino
Maver
G519
Jeko-1
Z-138
H
Primary MCLs
FGFR1 expression
NCL expression
n = 76
r = 0.57
P < 0.0001
I
RBD1
RBD2
RBD1
RBD2
FGFR1; 5' UTR (538-573)
J
Mino
Maver
#sh1
#sh2
Nucleolin
FGFR1
Myc
β-actin
Tet (5.0μg/mL)
K
Relative fold change (normalised to GAPDH)
CERS6-AS1
FGFR1
Mino
Maver
sh-Contol
sh1-Nucleolin
sh2-Nucleolin
L
% Inhibition
Mino
Maver
sh-Contol
sh-Nuc-1
sh-Nuc-2
M
sh-Contol
sh1-CERS6-AS1
sh2-CERS6-AS1
Mino
Maver
IC50
6.7 ± 0.09
2.6 ± 0.04
2.1 ± 0.12
> 10.0
3.4 ± 0.25
2.6 ± 0.44
% Inhibition
N6L (μM)
N
Mino (N6L; 5.0μM)
Maver (N6L; 5.0μM)
% Annexin-V (-) PI (-)
Tet (5.0μg/mL)
sh-Contol
sh1-CERS6-AS1
sh2-CERS6-AS1

Fig. 5 CERS6-AS1 and FGFR1 transcript interaction with nucleolin in MCL. (A) 3D cartoon showing CERS6-AS1 predicted G-triplex structure with nucleolin RBD3 and RBD4; IpTM and pTM values were 0.64 and 0.61 respectively (top panel). Surface view of CERS-AS1 G-triplex-Nucleolin complex (bottom panel). **(B)** RNA immunoprecipitation (RIP) analysis using α-nucleolin antibody in the absence or presence of nucleolin (RNA binding protein) targeting Nucant N6L demonstrated the interaction of CERS6-AS1 with nucleolin. Cells were treated with N6L at 10.0μM for 2.0 hours prior to lysis for RIP. Data here are showing the relative CERS6-AS1 interaction in nucleolin group compared to the IgG group. Ct value of the RIP output was normalized to their respective input Ct value. **(C)** Western blot was performed for input and RIP samples to detect nucleolin and actin expression in two MCL cell lines. **(D)** RIP analysis in the absence or presence of nucleolin targeting Nucant N6L or in CERS6-AS1 knockdown cells demonstrated the co-interaction of CERS6-AS1 and FGFR1 transcript with nucleolin protein. Cells were treated with N6L at 10.0μM for 2.0 hours prior to lysis for RIP. Ct value of the RIP output was normalized to their respective basal input Ct value. **(E)** Western blot for input and RIP samples was conducted to detect nucleolin and actin expression in accordance to the E. **(F)** Actinomycin D chase experiments determine FGFR1 transcript half-lives in Maver and Mino cell lines. Nucleolin inhibition or CERS6-AS1 knockdown significantly reduces the half-life of FGFR1 transcript. # denoted for statistical comparison between control vs N6L treated groups. **(G)** qRT-PCR data in the form of heatmap showing the relative expression ratio of CERS6-AS1, FGFR1, and nucleolin after treatment with N6L (1.0μM; 72 hours) vs non-treated (DMSO) MCL cells. A significant downregulation of FGFR1 was observed in all 6 MCL cell lines after N6L treatment. **(H)** Pearson correlation plot between FGFR1 vs nucleolin expression in primary MCL (n=76). Pearson correlation, two tailed $P < 0.0001$. **(I)** 3D cartoon model of the predicted nucleolin RBD1 and 2 with FGFR1 mRNA predicted stem loop structure through artificial intelligence; IpTM and pTM values 0.47 and 0.55 respectively (left panel). Surface view of FGFR1 stem loop-nucleolin complex (right panel). **(J)** Western blot analysis for nucleolin, FGFR1 and Myc in stable nucleolin knockdown cells generated (Mino and Maver). Tetracycline was added to induce the nucleolin shRNA expression at indicated dose for 72 hours before cell lysis. **(K)** Expression of CERS6-AS1 and FGFR1 at transcript level were detected by qRT-PCR in stable nucleolin knockdown cells. **(L)** Percentage growth inhibition shown by color matrix was detected by a WST-1 assay in nucleolin knockdown cells. The nucleolin shRNAs expression was induced by addition of tetracycline (5.0μg/mL) and cell viability was tested after 96 hours. **(M)** WST-1 cell metabolic activity assay was performed in CERS6-AS1 knockdown and sh-Control MCL cells after 72 hours of treatment with nucleolin inhibitor N6L at indicated doses. (* denoted comparison between sh-Control vs sh1-CERS6-AS1; and # denoted comparison between sh-Control vs sh2-CERS6-AS1). **(N)** CERS6-AS1 knockdown cells showed reduced cell survival and increased apoptosis as shown by the reduced percentage of annexin-V (-) PI (-) cells after N6L treatment (5.0μM; 72 hours). Groups were compared by two tailed unpaired Student's t-test; *$P < 0.05$, **$P < 0.01$, or ***$P < 0.001$*

Combining nucleolin inhibitor with FGFR1 targeting agent reduces stemness and induced cell death in MCL

Given the pivotal role of nucleolin and CERS6-AS1 in maintaining FGFR1 stability and sensitization to nucleolin targeting agent in CERS6-AS1 knockdown cells, we investigated therapeutic application of combining FGFR1 inhibitor erdafitinib with N6L in MCL. We treated six MCL cell lines with suboptimal concentrations (less than the IC50 value of the respective single agent) of erdafitinib and N6L and observed a significant synergistic combination effect with reduced MCL cell viability and increased apoptosis (Fig. 6A-B).

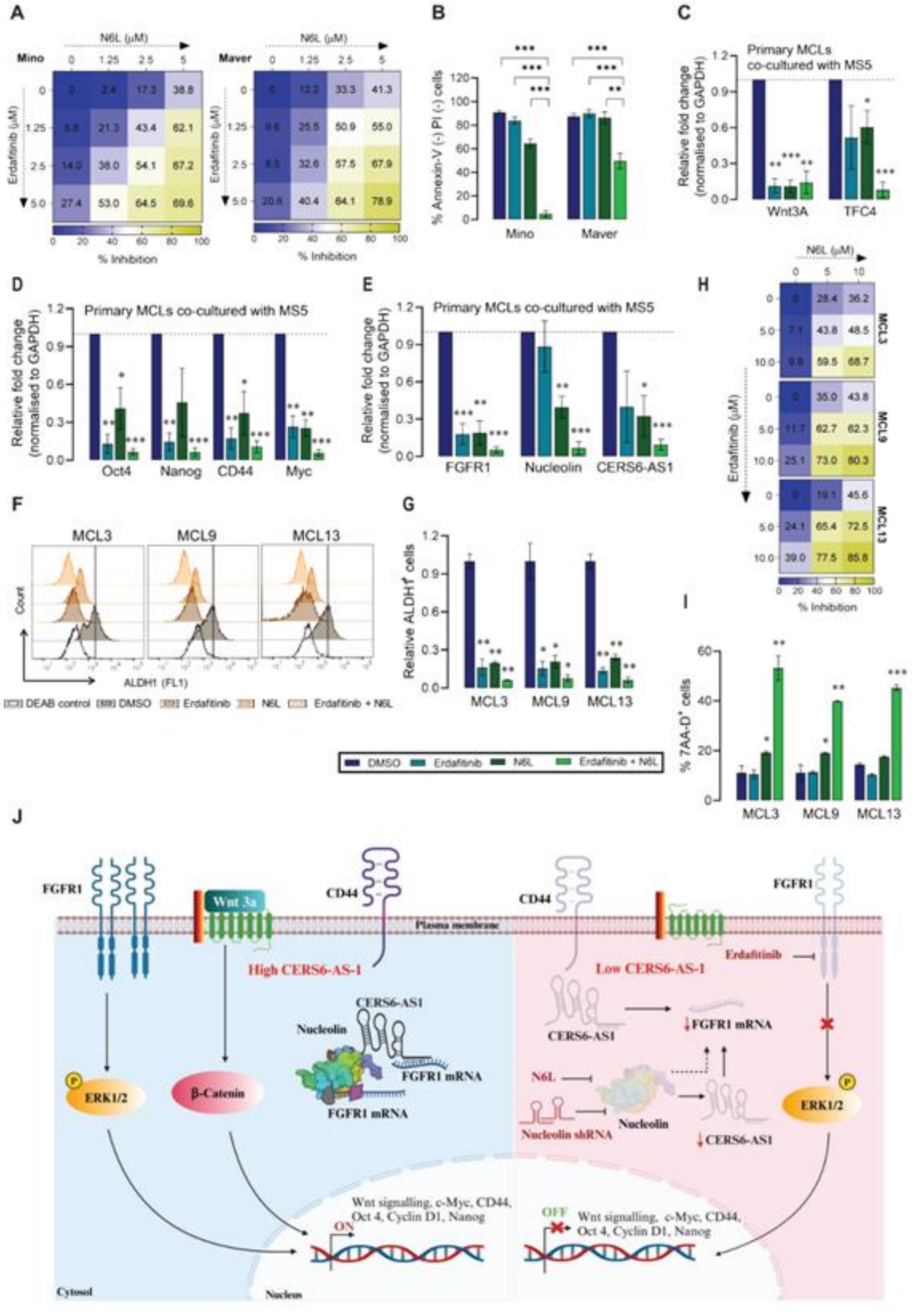
A
Mino
Maver
N6L (μM)
Erdafitinib (μM)
% Inhibition
B
% Annexin-V (-) PI (-) cells
Mino
Maver
C
Primary MCLs co-cultured with MS5
Relative fold change (normalised to GAPDH)
Wnt3A
TFC4
D
Primary MCLs co-cultured with MS5
Oct4
Nanog
CD44
Myc
E
Primary MCLs co-cultured with MS5
FGFR1
Nucleolin
CERS6-AS1
F
MCL3
MCL9
MCL13
Count
ALDH1 (FL1)
DEAB control
DMSO
Erdafitinib
N6L
Erdafitinib + N6L
G
Relative ALDH1+ cells
MCL3
MCL9
MCL13
DMSO
Erdafitinib
N6L
Erdafitinib + N6L
H
N6L (μM)
Erdafitinib (μM)
MCL3
MCL9
MCL13
% Inhibition
I
% 7AA-D+ cells
MCL3
MCL9
MCL13
J
FGFR1
Wnt 3a
CD44
Plasma membrane
High CERS6-AS-1
CERS6-AS1
Nucleolin
FGFR1 mRNA
ERK1/2
β-Catenin
Wnt signalling, c-Myc, CD44, Oct 4, Cyclin D1, Nanog
ON
Cytosol
Nucleus
CD44
FGFR1
Erdafitinib
Low CERS6-AS-1
CERS6-AS1
↓FGFR1 mRNA
N6L
Nucleolin
Nucleolin shRNA
↓CERS6-AS1
ERK1/2
OFF
Wnt signalling, c-Myc, CD44, Oct 4, Cyclin D1, Nanog

Fig. 6 Synergistic activity of combining nucleolin targeting agent with FGFR1 inhibitor in MCL. (A) Drug dose matrix data of MCL cells (Mino and Maver). The numbers in the matrix indicate the percentage of growth inhibition calculated by WST-1 assay after treated with indicated inhibitors for 72 hours (N6L and erdafitinib) either as single agents or in combination, relative to cells treated with a DMSO control. Data were visualized over the matrix using a color scale. **(B)** Combining N6L and erdafitinib (5.0μM each) increased MCL cell apoptosis, as shown by the reduced percentage of annexin-V (-) PI (-) cells in combination compared to single agent-treated cells for 72 hours. **(C)** Relative expression (qRT-PCR) of Wnt signaling markers (Wnt3A and TCF4); **(D)** stem cell markers (CD44, Oct4, Nanog); and **(E)** FGFR1, CERS6-AS1, and nucleolin in primary MCL samples (n=3) co-cultured with MS5 cells and treated with N6L or erdafitinib as single agents or in combination (1.0μM each; 7 days). **(F)** ALDH1 activity in primary MCL (n=3) co-cultured with MS5 cells after N6L or erdafitinib as single-agent or combination (1.0μM each; 7 days) using ALDEFLUOR kit and respective quantification shown as relative $ALDH1^+$ cells **(G)**. **(H)** Drug dose matrix data of primary MCL cells (n=3) grown with MS5 cells and treated with agents (N6L and erdafitinib) at indicated doses. The numbers in the matrix indicate the percentage of growth inhibition calculated by WST-1 assay after treated with indicated inhibitors for 72 hours. **(I)** Percentage of necrotic cells demonstrated by 7AA-D staining and flow cytometry in primary MCL (n=3) co-cultured with MS5 cells after N6L or erdafitinib as a single agent or combination (5.0μM each; 72 hours). **(J)** Model showing the role of CERS6-AS1/FGFR1 regulating loop in MCL. Each bar represents the mean ± SEM of three independent experiments. Groups were compared by two tailed unpaired Student's t-test; *$*P < 0.05$, **$*P < 0.01$, or ***$*P < 0.001$*

In addition, expression of cancer stem cell markers (CD44, Myc, Oct4, Nanog), Wnt signaling (TCF4 and Wnt3A), and respective FGFR1, nucleolin, and CERS6-AS1 levels were downregulated in combination compared to single agent treatment in MCL cell lines. Notably, this drug combination did not alter surface expression of chemo-immunotherapy targets (CD19, CD20; target of CAR T-cell therapy and monoclonal antibody rituximab respectively), suggesting combination compatibility with existing treatment modalities for MCL. We extended our investigation and tested the efficacy of combining nucleolin and FGFR1 targeting agents in patient-derived MCLs in our MS5 co-culture model. For this, we had selected three MCL patients with leukemic phase, where there was an abundance of tumor cells available (MCL3, MCL9, and MCL13). While there was no growth reduction or cytotoxicity to MS5 cells observed in either single agent or in combination, we observed erdafitinib treatment reduced growth of primary MCL, while N6L treatment attenuated their adhesion to stromal layer. As a single agent, erdafitinib treatment alone significantly abrogated the percentage of drug-resistant $CD45^+CD19^{low}$ MCL cells. Notably, combination of erdafitinib and N6L showed significant effects on MCL cells, including downregulation of cancer stem cell markers, Wnt signaling genes, and expression of FGFR1, CERS6-AS1 and nucleolin in primary MCL cells in co-culture system (Fig 6C-E). Notably, combining N6L with erdafitinib led to reduction in percentage of ALDH1+ MCL cells accompanied by reduced MCL cell viability and induced significant cell death (Fig 6F-I). These findings underscore the potential of combining nucleolin-targeting and FGFR1-targeting agents as a promising therapeutic strategy for MCL (Fig. 6J).

Statistical analysis:

Clinicopathologic features were analysed using the Fisher exact test. Overall survival (OS) was determined using Kaplan–Meier analyses and a log-rank test. All the data were analysed using GraphPad Prism 8.0 software (San Diego, CA, USA). Results were presented as mean ±

standard deviation (SD) of the three independent experiments. Differences between the groups were compared using a two-tailed unpaired Student's t-test, and *P < 0.05* was considered statistically significant. Significance levels were denoted as follows: **P < 0.05, **P < 0.01, or ***P < 0.001*.

Discussion:

In MCL, a number of lncRNAs such as MALAT1, ROR1-AS1, FOXP4-AS1, GATA6-AS, and MORT have demonstrated their oncogenic or tumor-suppressive properties (21-25, 48, 49). However, importance of lncRNAs in context of MCL-TME interaction remains unexplored. Here, we have employed clinical samples from multiple hospitals of different regions in India and assessed the expression and functional importance of lncRNA CERS6-AS in MCL. CERS6-AS1 was first reported in breast cancer (2020), where its overexpression was positively correlated with malignant phenotype (34). After that, within past three years, its expression and functions have been documented in multiple solid tumors (50-53). CERS6-AS1 regulates tumor development and progression by acting as signals sequestering miRNA, and suppressing their inhibitory effects on critical molecular targets. To date, CERS6-AS1 has been unexplored in liquid cancer and, like other lncRNA, has not been explored in oncogenic tumor-stromal cells cross-talks. In this study, we have investigated expression and functional significance of CERS6-AS1 in MCL, shedding light on its potential role in MCL pathogenesis. Our findings revealed that CERS6-AS1 is upregulated in patient-derived MCL compared to normal B-cells or naïve B-cells, and associated with clinically poor overall survival. Upregulation of CERS6-AS1 in MCL is consistent with its previously reported oncogenic functions in solid tumors. Our study expands on these findings by demonstrating its involvement in liquid cancers, particularly in MCL, highlighting its versatility across different cancer types.

MCL is considered an incurable subtype of B-cell lymphoma with significant bone marrow involvement (60-80%). Despite of multiple treatment options, high rates of MCL relapse cases suggests its incomplete elimination. This implicates the presence of MCL-subsets with inherited or acquired tumor-initiating (TI) properties attained within the protective microenvironments. Few studies till date have demonstrated the presence MCL-subsets that require stromal cell interaction for survival and express differential stem cell signatures. Using four primary MCLs, Brennan et al being first demonstrated small population of ALDH+ cells were highly clonogenic, relatively quiescent, and showed resistant to chemotherapeutic agent (54). Second study by Chen et al had isolated MCL-initiating cells (MCL-ICs) based on lack of surface CD19 expression, and as few as 100 of these cells could form tumor in immunocompromised mice (55). Similar observation was published by Medina et al., where CD19-CD133+ MCL cells had tumor-forming ability and exhibited self-renewal properties (35). But these studies lacked mechanistic angle that could led to therapeutically target TI-MCL cells. Later, Mathur et al had characterized MCL-ICs and identified these tumor subsets can be targetable by Wnt inhibitors (5). Though Wnt inhibitors are effective in killing these TI-cells, such inhibitors also have disadvantages as they deplete tissues resident normal stem cell population and posing challenges in clinical translation (56, 57). All these studies have clearly shown, the importance of MCL-stromal cells interactions. But to date, we lacked a therapeutic target that could abolish this oncogenic cross-talk in MCL. Our observation is consistent with a previous report that shows an upregulation of the stemness behavior of MCL when cultured on stromal

layer (11). Our study has further explored the intricate interplay between MCL and stromal cells, and we noted a significant upregulation of CERS6-AS1 expression can be regulated by stromal cells, thus postulating that both cell intrinsic and extrinsic factors could contribute to CERS6-AS1 expression in MCL. Within the stromal cell microenvironment, a subset of MCL adhered to the stromal cells layer; those directly receive growth and survival signals via adhesion molecules, and cytokines that facilitate global differences in key signaling pathways (15, 58). With this notion, our patient-derived MCL adhered to stromal cells showed a significant upregulation of CERS6-AS1 expression with consistent changes in the level of cancer stem cell genes (CD44 and Nanog) and resistance to BTK inhibitors than MCL cells grown in suspension.

FGFR1 activation or amplification is a known driver of tumorigenesis in multiple cancers (41, 59-61). Moreover, enhanced FGFR signaling can also lead to the activation of several downstream oncogenic pathways, among which the PI3K/AKT, RAS/MAPK, JAK/STAT, and PLCγ pathways are prominent. FGFR1 signaling can enhance the expression of transcription factors and genes associated with stemness, such as Oct4, Sox2, and Nanog (38, 62, 63). FGFR1 has emerged as an essential player in MCL pathogenesis and progression, as highlighted by recent studies (13, 64). In the present study, we found a significant increase in FGFR1 expression in MCL when grown with stromal cells, in adherent-MCL than in suspension-MCL and in $CD45^{+}CD19^{low}$ cells than $CD45^{+}CD19^{high}$ MCL cells. Also, FGFR1 expression was positively correlated with CERS6-AS1 expression. The observed high level of FGFR1 in multiple sets of experiments and its consistent positive correlation with CERS6-AS1 expression suggests a potential functional relationship between these two molecules that was confirmed in our CERS6-AS1 knockdown cells where a significant downregulation of FGFR1 and downstream signaling consistent to prior report was observed (13).

LncRNAs primarily function through various mechanisms, and one significant mode of action is interacting with RBPs. Through in-silico and *in vitro* study, we found nucleolin interaction with CERS6-AS1, which was inhibited by a nucleolin targeting nucant N6L. The observed inhibition of nucleolin interaction with CERS6-AS1 by N6L, corroborates specificity of nucleolin-CERS6-AS1 interaction. We further found that CERS6-AS1 mediates nucleolin interaction with FGFR1 transcript, and appears to enhance its stability, thereby could potentially influencing FGFR1 levels and downstream signaling “MYC-EZH2-CDKNIC” pathways (13). These findings score importance of post-transcriptional regulatory mechanisms mediated by CERS6-AS1 in fine-tuning FGFR1 expression. Nucleolin is upregulated in various solid and liquid cancer and is uniquely localized on surface of cancer cells, a phenomenon not observed in normal cells and that’s makes it an appealing target for therapeutic intervention (65-67). The positive correlation between nucleolin and FGFR1 expression in patient-derived MCL cells suggests a potential clinical relevance of the nucleolin-FGFR1 axis in MCL. In addition, the observed downregulation of FGFR1 expression at RNA level upon N6L treatment or nucleolin knockdowns that provided further evidence for nucleolin-dependent activation of FGFR1 associated oncogenic axis.

Our informatics and computational study established that nucleolin binds with CERS6-AS1 specifically “1057-1079” bases which is predicted to adopt G-triplex structure preferably with RBD3 and RBD4. Additionally, our results further establishes that nucleolin RBD1 and RBD2 domains interacts with FGFR1 mRNA through it’s 5’UTR spanning “538-573”

bases which adopts stem loop structures. The published crystal structures of nucleolin's RBD1 and RBD2 binding to stem loop structure of another RNA reported previously validate our observation (68). Based on our omics data and *in vitro* changes in FGFR1 expression after nucleolin inhibition, we also believe that nucleolin is directly interacting with FGFR1 transcript and thereby maintaining FGFR1 stability, which may contribute to elevated FGFR1 expression in MCL. Given that CERS6-AS1 has been identified as a sponge of miRNA, there remains the possibility that CERS6-AS1-associated miRNAs could also play a role in FGFR1 downregulation in our MCL model which has not been tested in this study. Based on previously reported observation and follow up our computational investigation, this is found that CERS6-AS1 lncRNA regulates the microRNA-15a-5p/FGFR1 axis to facilitate the oncogenicity (27). Further investigations are required to understand how CERS6-AS1 expression is regulated in MCL. Shading lights towards this, we observed a significant downregulation of CERS6-AS1 in our nucleolin knockdown clones indicating its nucleolin dependent expression regulation that further required investigations. We combined N6L with FGFR1 targeting agent erdafitinib (Balversa) that recently received (January 19, 2024), FDA approved for the treatment of adult patients with locally advanced or metastatic urothelial carcinoma. Our data showed that combining both drugs have a synergistic effect in 6 MCL cell lines, 3 primary MCLs and also reduced stem cell signatures and induced cell death.

In summary, our study demonstrates that CERS6-AS1 expression has prognostic value in MCL but this should be confirmed in an independent cohort. The gained expression of CERS6-AS1 in the presence of a stromal layer suggests a context-dependent regulation of this lncRNA in the microenvironment. Our results reveal that upregulation of the oncogenic FGFR1-Myc axis in MCL is a consequence of increased expression of CERS6-AS1 and nucleolin protein. In addition, the identification of nucleolin as an RNA-binding protein that regulates FGFR1 transcript stability via a direct interaction and co-binding to CERS6-AS1 provides mechanistic insights into the regulatory network controlling FGFR1 expression in MCL. We discovered a synergistic impact of combining a nucleolin-targeting agent with erdafitinib, a FGFR inhibitor. This suggests that combinatorial therapeutic strategies targeting multiple components of this axis may offer enhanced efficacy in MCL treatment. In conclusion, our preclinical study highlights the clinical relevance of targeting the nucleolin-CERS6-AS1-FGFR1 axis in MCL.

Impact of the research in the advancement of knowledge or benefit to mankind:

Our study has identified molecular signatures related to stemness in mantle cell lymphoma, which is an aggressive form of B cell neoplasm. With the help of a smaller population of cancer stem cells, we have found cell surface protein FGFR1 and nucleolin, those are particularly helping the aggressiveness, stemness and rest signatures to this B cell lymphoma, through a long non-coding RNA, CERS6-AS1. Through multiple experiment our study proposes that targeting these cancer stem cell associated signature in conjecture with the current chemotherapy will provide a significant advancement in the treatment and survival benefit.

Beyond MCL, the broader implications of our research suggest that the CERS6-FGFR1 axis may be relevant in other malignancies, offering hope for more effective treatments across various cancers. This could ultimately lead to enhanced survival rates and improved quality of life for many patients. By deepening our understanding of the tumor microenvironment and its influence on cancer progression, this research contributes to the ongoing fight against cancer, with the potential to benefit not only MCL patients but also those suffering from other refractory or relapsed cancers. This work is a step forward in the global effort to reduce the burden of cancer and improve the lives of countless individuals.

References:

1. Vose JM. Mantle cell lymphoma: 2013 Update on diagnosis, risk-stratification, and clinical management. Am J Hematol. 2013;88(12):1082-8.

2. Jain N, Mamgain M, Chowdhury SM, Jindal U, Sharma I, Sehgal L, et al. Beyond Bruton's tyrosine kinase inhibitors in mantle cell lymphoma: bispecific antibodies, antibody-drug conjugates, CAR T-cells, and novel agents. J Hematol Oncol. 2023;16(1):99.

3. Avyakta Kallam M, Vose JM. Current Treatments in Mantle Cell Lymphoma. Oncology (Williston Park). 2023;37(8):326-33.

4. Bukhari A, El Chaer F, Koka R, Singh Z, Hutnick E, Ruehle K, et al. Rapid relapse of large B-cell lymphoma after CD19 directed CAR-T-cell therapy due to CD-19 antigen loss. Am J Hematol. 2019;94(10):E273-E5.

5. Mathur R, Sehgal L, Braun FK, Berkova Z, Romaguerra J, Wang M, et al. Targeting Wnt pathway in mantle cell lymphoma-initiating cells. J Hematol Oncol. 2015;8:63.

6. Kumar A, Sha F, Toure A, Dogan A, Ni A, Batlevi CL, et al. Patterns of survival in patients with recurrent mantle cell lymphoma in the modern era: progressive shortening in response duration and survival after each relapse. Blood Cancer J. 2019;9(6):50.

7. George B, Chowdhury SM, Hart A, Sircar A, Singh SK, Nath UK, et al. Ibrutinib Resistance Mechanisms and Treatment Strategies for B-Cell lymphomas. Cancers (Basel). 2020;12(5).

8. Konopleva MY, Jordan CT. Leukemia stem cells and microenvironment: biology and therapeutic targeting. J Clin Oncol. 2011;29(5):591-9.

9. Le Bris Y, Normand A, Bouard L, Menard A, Bossard C, Moreau A, et al. Aggressive, early resistant and relapsed mantle cell lymphoma distinct extrinsic microenvironment highlighted by transcriptome analysis. EJHaem. 2022;3(4):1165-71.

10. Esmeray Sonmez E, Hatipoglu T, Kursun D, Hu X, Akman B, Yuan H, et al. Whole Transcriptome Sequencing Reveals Cancer-Related, Prognostically Significant Transcripts and Tumor-Infiltrating Immunocytes in Mantle Cell Lymphoma. Cells. 2022;11(21).

11. Medina DJ, Goodell L, Glod J, Gelinas C, Rabson AB, Strair RK. Mesenchymal stromal cells protect mantle cell lymphoma cells from spontaneous and drug-induced apoptosis through secretion of B-cell activating factor and activation of the canonical and non-canonical nuclear factor kappaB pathways. Haematologica. 2012;97(8):1255-63.

12. Jain P, Nomie K, Kotlov N, Segodin V, Hill H, Ok CY, et al. Immune-depleted tumor microenvironment is associated with poor outcomes and BTK inhibitor resistance in mantle cell lymphoma. Blood Cancer J. 2023;13(1):156.

13. Sircar A, Singh S, Xu-Monette ZY, Coyle KM, Hilton LK, Chavdoula E, et al. Exploiting the fibroblast growth factor receptor-1 vulnerability to therapeutically restrict the MYC-EZH2-CDKN1C axis-driven proliferation in Mantle cell lymphoma. Leukemia. 2023;37(10):2094-106.

14. Araujo-Ayala F, Dobano-Lopez C, Valero JG, Nadeu F, Gava F, Faria C, et al. A novel patient-derived 3D model recapitulates mantle cell lymphoma lymph node signaling, immune profile and in vivo ibrutinib responses. Leukemia. 2023;37(6):1311-23.

15. Sadeghi L, Wright APH. GSK-J4 Inhibition of KDM6B Histone Demethylase Blocks Adhesion of Mantle Cell Lymphoma Cells to Stromal Cells by Modulating NF-kappaB Signaling. Cells. 2023;12(15).

16. Pandey PR, Young KH, Kumar D, Jain N. RNA-mediated immunotherapy regulating tumor immune microenvironment: next wave of cancer therapeutics. Mol Cancer. 2022;21(1):58.

17. Liu L, Wang Q, Qiu Z, Kang Y, Liu J, Ning S, et al. Noncoding RNAs: the shot callers in tumor immune escape. Signal Transduct Target Ther. 2020;5(1):102.

18. Winkle M, El-Daly SM, Fabbri M, Calin GA. Noncoding RNA therapeutics - challenges and potential solutions. Nat Rev Drug Discov. 2021;20(8):629-51.

19. Gholami A, Farhadi K, Sayyadipour F, Soleimani M, Saba F. Long noncoding RNAs (lncRNAs) in human lymphomas. Genes Dis. 2022;9(4):900-14.

20. Khanmohammadi S, Fallahtafti P. Long non-coding RNA as a novel biomarker and therapeutic target in aggressive B-cell non-Hodgkin lymphoma: A systematic review. J Cell Mol Med. 2023;27(14):1928-46.

21. Hu G, Gupta SK, Troska TP, Nair A, Gupta M. Long non-coding RNA profile in mantle cell lymphoma identifies a functional lncRNA ROR1-AS1 associated with EZH2/PRC2 complex. Oncotarget. 2017;8(46):80223-34.

22. Wang X, Sehgal L, Jain N, Khashab T, Mathur R, Samaniego F. LncRNA MALAT1 promotes development of mantle cell lymphoma by associating with EZH2. J Transl Med. 2016;14(1):346.

23. Tao HF, Shen JX, Hou ZW, Chen SY, Su YZ, Fang JL. lncRNA FOXP4-AS1 predicts poor prognosis and accelerates the progression of mantle cell lymphoma through the miR-423-5p/NACC1 pathway. Oncol Rep. 2021;45(2):469-80.

24. Fan Z, Wang X, Li P, Mei C, Zhang M, Zhao C. Overexpression of lncRNA GATA6-AS inhibits cancer cell proliferation in mantle cell lymphoma by downregulating GLUT1. Oncol Lett. 2019;18(3):2443-7.

25. Tang X, Long Y, Xu L, Yan X. LncRNA MORT Inhibits Cancer Cell Proliferation and Promotes Apoptosis in Mantle Cell Lymphoma by Upregulating miRNA-16. Cancer Manag Res. 2020;12:2119-25.

26. Rastad H, Samimisedeh P, Alan MS, Afshar EJ, Ghalami J, Hashemnejad M, et al. The role of lncRNA CERS6-AS1 in cancer and its molecular mechanisms: A systematic review and meta-analysis. Pathol Res Pract. 2023;241:154245.

27. Yun Z, Meng F, Li S, Zhang P. Long non-coding RNA CERS6-AS1 facilitates the oncogenicity of pancreatic ductal adenocarcinoma by regulating the microRNA-15a-5p/FGFR1 axis. Aging (Albany NY). 2021;13(4):6041-54.

28. Xu J, Wang J, He Z, Chen P, Jiang X, Chen Y, et al. LncRNA CERS6-AS1 promotes proliferation and metastasis through the upregulation of YWHAG and activation of ERK signaling in pancreatic cancer. Cell Death Dis. 2021;12(7):648.

29. Xu B, Wei Y, Liu F, Li L, Zhou S, Peng Y, et al. Long noncoding RNA CERS6-AS1 modulates glucose metabolism and tumor progression in hepatocellular carcinoma by promoting the MDM2/p53 signaling pathway. Cell Death Discov. 2022;8(1):348.

30. Li Z, Liu X, Luo N, Pang Y, Hou Y, Jiang G. Long non-coding RNA CERS6-AS1 plays a prognostic role in promoting the progression of gastric cancer. Bioengineered. 2021;12(2):12931-9.

31. Zhao SY, Wang Z, Wu XB, Zhang S, Chen Q, Wang DD, et al. CERS6-AS1 contributes to the malignant phenotypes of colorectal cancer cells by interacting with miR-15b-5p to regulate SPTBN2. Kaohsiung J Med Sci. 2022;38(5):403-14.

32. Cabaret O, Perron E, Bressac-de Paillerets B, Soufir N, de la Fouchardiere A. Occurrence of BAP1 germline mutations in cutaneous melanocytic tumors with loss of BAP1-expression: A pilot study. Genes Chromosomes Cancer. 2017;56(9):691-4.

33. Gao KF, Zhao YF, Liao WJ, Xu GL, Zhang JD. CERS6-AS1 promotes cell proliferation and represses cell apoptosis in pancreatic cancer via miR-195-5p/WIPI2 axis. Kaohsiung J Med Sci. 2022;38(6):542-53.

34. Bao G, Huang J, Pan W, Li X, Zhou T. Long noncoding RNA CERS6-AS1 functions as a malignancy promoter in breast cancer by binding to IGF2BP3 to enhance the stability of CERS6 mRNA. Cancer Med. 2020;9(1):278-89.

35. Medina DJ, Abass-Shereef J, Walton K, Goodell L, Aviv H, Strair RK, et al. Cobblestone-area forming cells derived from patients with mantle cell lymphoma are enriched for CD133+ tumor-initiating cells. PLoS One. 2014;9(4):e91042.

36. Du S, Zhang Y, Xu J. Current progress in cancer treatment by targeting FGFR signaling. Cancer Biol Med. 2023;20(7):490-9.

37. Wiedlocha A, Haugsten EM, Zakrzewska M. Roles of the FGF-FGFR Signaling System in Cancer Development and Inflammation. Cells. 2021;10(9).

38. Ko J, Meyer AN, Haas M, Donoghue DJ. Characterization of FGFR signaling in prostate cancer stem cells and inhibition via TKI treatment. Oncotarget. 2021;12(1):22-36.

39. Loda A, Calza S, Giacomini A, Ravelli C, Krishna Chandran AM, Tobia C, et al. FGF-trapping hampers cancer stem-like cells in uveal melanoma. Cancer Cell Int. 2023;23(1):89.

40. Bi Y, Zheng R, Hu J, Shi R, Shi J, Wang Y, et al. A novel FGFR1 inhibitor CYY292 suppresses tumor progression, invasion, and metastasis of glioblastoma by inhibiting the Akt/GSK3beta/snail signaling axis. Genes Dis. 2024;11(1):479-94.

41. Cheng Q, Ma Z, Shi Y, Parris AB, Kong L, Yang X. FGFR1 Overexpression Induces Cancer Cell Stemness and Enhanced Akt/Erk-ER Signaling to Promote Palbociclib Resistance in Luminal A Breast Cancer Cells. Cells. 2021;10(11).

42. Shaath H, Vishnubalaji R, Elango R, Kardousha A, Islam Z, Qureshi R, et al. Long non-coding RNA and RNA-binding protein interactions in cancer: Experimental and machine learning approaches. Semin Cancer Biol. 2022;86(Pt 3):325-45.

43. Wu R, Li L, Bai Y, Yu B, Xie C, Wu H, et al. The long noncoding RNA LUCAT1 promotes colorectal cancer cell proliferation by antagonizing Nucleolin to regulate MYC expression. Cell Death Dis. 2020;11(10):908.

44. Aguilar-Garrido P, Otero-Sobrino A, Navarro-Aguadero MA, Velasco-Estevez M, Gallardo M. The Role of RNA-Binding Proteins in Hematological Malignancies. Int J Mol Sci. 2022;23(17).

45. Wise JF, Berkova Z, Mathur R, Zhu H, Braun FK, Tao RH, et al. Nucleolin inhibits Fas ligand binding and suppresses Fas-mediated apoptosis in vivo via a surface nucleolin-Fas complex. Blood. 2013;121(23):4729-39.

46. Jain N, Zhu H, Khashab T, Ye Q, George B, Mathur R, et al. Targeting nucleolin for better survival in diffuse large B-cell lymphoma. Leukemia. 2018;32(3):663-74.

47. Carvalho LS, Goncalves N, Fonseca NA, Moreira JN. Cancer Stem Cells and Nucleolin as Drivers of Carcinogenesis. Pharmaceuticals (Basel). 2021;14(1).

48. Guo Y, Xie Y, Luo Y. The Role of Long Non-Coding RNAs in the Tumor Immune Microenvironment. Front Immunol. 2022;13:851004.

49. Pi YN, Qi WC, Xia BR, Lou G, Jin WL. Long Non-Coding RNAs in the Tumor Immune Microenvironment: Biological Properties and Therapeutic Potential. Front Immunol. 2021;12:697083.

50. Zhang J, Lou W. A Key mRNA-miRNA-lncRNA Competing Endogenous RNA Triple Sub-network Linked to Diagnosis and Prognosis of Hepatocellular Carcinoma. Front Oncol. 2020;10:340.

51. Zhou C, Chen Y, He X, Zheng Z, Xue D. Functional Implication of Exosomal miR-217 and miR-23b-3p in the Progression of Prostate Cancer. Onco Targets Ther. 2020;13:11595-606.

52. Yu H, Pang Z, Li G, Gu T. Bioinformatics analysis of differentially expressed miRNAs in non-small cell lung cancer. J Clin Lab Anal. 2021;35(2):e23588.

53. Fan YX, Shi HY, Hu YL, Jin XL. Circ_0000144 facilitates the progression of thyroid cancer via the miR-217/AKT3 pathway. J Gene Med. 2020;22(12):e3269.

54. Brennan SK, Meade B, Wang Q, Merchant AA, Kowalski J, Matsui W. Mantle cell lymphoma activation enhances bortezomib sensitivity. Blood. 2010;116(20):4185-91.

55. Chen Z, Ayala P, Wang M, Fayad L, Katz RL, Romaguera J, et al. Prospective isolation of clonogenic mantle cell lymphoma-initiating cells. Stem Cell Res. 2010;5(3):212-25.

56. Pattabiraman DR, Weinberg RA. Tackling the cancer stem cells - what challenges do they pose? Nat Rev Drug Discov. 2014;13(7):497-512.

57. Turdo A, Veschi V, Gaggianesi M, Chinnici A, Bianca P, Todaro M, et al. Meeting the Challenge of Targeting Cancer Stem Cells. Front Cell Dev Biol. 2019;7:16.

58. Sadeghi L, Arvidsson G, Merrien M, A MW, Gorgens A, Smith CIE, et al. Differential B-Cell Receptor Signaling Requirement for Adhesion of Mantle Cell Lymphoma Cells to Stromal Cells. Cancers (Basel). 2020;12(5).

59. Pacini L, Jenks AD, Lima NC, Huang PH. Targeting the Fibroblast Growth Factor Receptor (FGFR) Family in Lung Cancer. Cells. 2021;10(5).

60. Bi Y, Zheng R, Hu J, Shi R, Shi J, Wang Y, et al. Corrigendum to "A novel FGFR1 inhibitor CYY292 suppresses tumor progression, invasion, and metastasis of glioblastoma by inhibiting the Akt/GSK3beta/snail signaling axis" [Genes & Diseases 11 (2024) 479-494]. Genes Dis. 2024;11(3):101168.

61. Dhangar S, Shanmukhaiah C, Sawant L, Ghatanatti J, Shah A, Mathan SL, et al. Synergetic effect of Azacitidine and Sorafenib in treatment of a case of myeloid neoplasm with sole chromosomal abnormality t(8;22)(p11.2;q11.2)/BCR-FGFR1 rearrangement. Cancer Genet. 2023;274-275:26-9.

62. Yamamoto T, Miyoshi H, Kakizaki F, Maekawa H, Yamaura T, Morimoto T, et al. Chemosensitivity of Patient-Derived Cancer Stem Cells Identifies Colorectal Cancer Patients with Potential Benefit from FGFR Inhibitor Therapy. Cancers (Basel). 2020;12(8).

63. Feng W, Gao M, Yang M, Li X, Gan Z, Wu T, et al. TNFAIP3 promotes ALDH-positive breast cancer stem cells through FGFR1/MEK/ERK pathway. Med Oncol. 2022;39(12):230.

64. Zhang L, Yao Y, Zhang S, Liu Y, Guo H, Ahmed M, et al. Metabolic reprogramming toward oxidative phosphorylation identifies a therapeutic target for mantle cell lymphoma. Sci Transl Med. 2019;11(491).

65. Thongchot S, Aksonnam K, Thuwajit P, Yenchitsomanus PT, Thuwajit C. Nucleolin-based targeting strategies in cancer treatment: Focus on cancer immunotherapy (Review). Int J Mol Med. 2023;52(3).

66. Romano S, Fonseca N, Simoes S, Goncalves J, Moreira JN. Nucleolin-based targeting strategies for cancer therapy: from targeted drug delivery to cytotoxic ligands. Drug Discov Today. 2019;24(10):1985-2001.

67. Ferrara B, Belbekhouche S, Habert D, Houppe C, Vallee B, Bourgoin-Voillard S, et al. Cell surface nucleolin as active bait for nanomedicine in cancer therapy: a promising option. Nanotechnology. 2021;32(32).

68. Allain FH, Bouvet P, Dieckmann T, Feigon J. Molecular basis of sequence-specific recognition of pre-ribosomal RNA by nucleolin. EMBO J. 2000;19(24):6870-81.